Mineralogical Effects on Organic Detectability in Mars Analog Sediments

Madeline Raith[1]

Advisors: Dr. Ricardo Arevalo Jr.[1], Dr. Michael Thorpe[1,2], Ashley M. Hanna[1]

GEOL 394 Final Report

April 25th, 2023

Affiliations: [1]University of Maryland, [2]NASA Goddard Space Flight Center

0.0 Abstract

Mars exploration is a dominant part of active planetary research with goals including understanding past and present geologic surface processes and searching for chemical signs of life. Like much of the red planet's surface, Lake Sandvatn in southwest Iceland shares a basaltic terrain; fluvial, deltaic, and lacustrine environments; and a cold climate, making it a potential analog site for understanding martian surface processes. In order to provide a reference frame for observations on Mars, this study compares the modal mineralogy of sediments derived from the Lake Sandvatn watershed to the mineralogy of Gale crater, Mars as inferred from in situ observations collected by the Curiosity rover. Based on X-ray diffraction measurements that mimic the experiments conducted by the CheMin instrument on Curiosity, Lake Sandvatn and Gale crater are both composed predominantly of plagioclase, pyroxene, olivine, and amorphous material; the presence of clay minerals is less comparable between the two sites. To investigate the role of mineralogy on the detectability of prospective chemical biosignatures on Mars, proxies for the individual mineral phases observed in the highest modal abundances, namely augite, labradorite, olivine, and montmorillonite, are doped with cholesterol and betulinic acid and analyzed via laser desorption mass spectrometry (LDMS). Analyses of cholesterol were well above the background for many tested molarities across all four mineral references, however, betulinic acid did not often produce peaks above the background. The limits of detection for cholesterol adsorbed onto each of these phases are calculated via linear regression analysis of a sensitivity curve. Based on the data set collected here, olivine has the highest inferred limit of detection at 0.00021 M and montmorillonite has the lowest limit of detection at 0.00003 M. Overall, the results from this study showed minerals present on Mars can also be produced in similar quantities in an analog environment, and these minerals will play a crucial role in variations on the detectability of potential biosignatures.

0.1 Plain Language Summary

Mars is one of the most explored planetary bodies in our solar system, yet there is still more to learn about its past environment and, if life arose, whether fingerprints of that life might be preserved in the rock record. This study focuses on using Lake Sandvatn in southwest Iceland, a location with broad geologic similarities to Mars and a colder climate, to understand how the minerals present in a Mars-like environment can affect the ability to detect signs of life. First, the mineralogy at Lake Sandvatn was characterized using X-ray diffraction to provide a reference frame for basaltic terrains. This data was compared to data from Mars to determine how similar the mineralogy is and to identify limitations of using Lake Sandvatn as an analog. Then, mineral reference materials were used to characterize the detectability of two biologically relevant organic molecules that may serve as potential chemical signatures of life in the rock record, cholesterol and betulinic acid. The major minerals at Lake Sandvatn and on Mars include plagioclase, pyroxene, olivine, and clay. The two lipids were added to these minerals and measured using laser desorption mass spectrometry, a technique that will be used in future spaceflight missions. The results presented here showed that clay produces the greatest signal intensity of cholesterol and betulinic acid at higher concentrations, and at lower concentrations, all minerals have similar signal intensities. Using these results a limit of detection, where samples doped with a lower concentration would not produce visible signal, was inferred for each mineral which showed olivine had the highest limit of detection and clay had the lowest limit of detection. This work serves to inform on the role minerals will play in potentially detecting life on other planets.

1. Introduction

Life detection and the identification of habitable environments in our solar system are two focal topics of the planetary science community. The Planetary Science and Astrobiology Decadal Survey (2023–2032), a document that is produced as a guide for NASA's Planetary Science and Astrobiology priorities based on community input, has prioritized understanding: i) the conditions under which life evolved and survived on Earth; ii) how environments on other planetary bodies may or may not be habitable for life as we know it; and, iii) how we can detect past or present signs of life if is present (Committee on the Planetary Science and Astrobiology Decadal Survey et al., 2022). In addition to such objectives, which are focused on astrobiology, another priority for future research is constraining how processes at the surface and subsurface have shaped planetary bodies, and how these processes could influence local habitability. This includes understanding the depositional environments and geologic context shaping other planets over time.

Currently, there are ten missions actively exploring Mars: two rovers, one lander, and seven orbiters from NASA, ESA, MBRSC, and CNSA combined. Numerous successful missions have made it to Mars, making it the third most explored planetary body after only the Moon and Earth. Past missions initially focused on characterizing the general geology, climate, and chemistry of the planet (Hubbard et al., 2002). The NASA Sojourner rover onboard the Pathfinder lander observed rounded pebbles and conglomerates indicating fast flowing water on the surface of Mars in the past (Team, 1997). Missions following Pathfinder continued to search for signs of water, resulting in strong evidence for free water in Mars' geologic past based on observations ranging from geomorphological structures (e.g., Baker, 2006) to radar observations of water beneath the polar caps (e.g., Orosei et al., 2018). More recently, the primary goals of the NASA Mars Exploration program are to search for signs of life and understand the potential habitability of Mars, two objectives that the Perseverance and Curiosity rovers are actively undertaking, respectively. There are future missions in development around the world (e.g., ESA ExoMars Rosalind Franklin Rover) set to fly to Mars in the next decade, demonstrating that Mars exploration is still a dominant focus in planetary exploration (Vago et al., 2017).

The martian environment has evolved significantly over time. While there is now definitive evidence for water on Mars, as described briefly above, there is debate about the quantity, duration, and climate in which the water was present. Earlier climate models suggested some combination of warm or cold and wet or dry early Mars (e.g. Fairén, 2010; Haberle, 1998; Pollack et al., 1987). However, recent models suggest the early Mars environment was cold and arid at the surface with intermittent periods of warming and transient surface water based on the presence of surface clay minerals (Ehlmann et al., 2011; Wordsworth, 2016). Today, the subsurface is proposed to be a more habitable environment due to shielding from solar and galactic cosmic rays, a positive thermal gradient, and less oxidative conditions compared to the perchlorate-rich surface (Atri, 2020; Tarnas et al., 2021). Furthermore, the presence of minerals such as chlorite indicates a potentially warmer habitable subsurface environment with hydrothermal groundwater circulation (Ehlmann et al., 2011). Whether life arose early in Mars' history or more recently, evidence for biological activity could be preserved in the rock record. Curiosity and Perseverance are actively exploring craters where millions of years of the rock record have been exposed. In particular, the Curiosity rover has been observing the rock record in Gale crater, which spans over the first hundreds of millions of years of Mars (Wray, 2013). This rock record shows evidence of changing environments including lacustrine, fluvial, deltaic, and aeolian (Grotzinger et al., 2015).

Future spaceflight missions, such as ExoMars, are set to explore Mars in search of chemical indicators of present and/or past life in the form of biosignatures (Vago et al., 2017). Biosignatures are defined by the Planetary Science and Astrobiology Decadal Survey as "any characteristic, element, molecule, substance, or feature that can be used as evidence for past or present life." (Committee on the Planetary Science and Astrobiology Decadal Survey et al., 2022). Biosignatures come in many forms, including laminae produced by stromatolites, biogenic minerals (i.e. mollusks reinforcing their shells with calcium carbonate), and refractory organic macromolecules. One class of biological macromolecule that is of particular interest to the community is lipids, which are insoluble in water; lipids may be more resistant to breakdown during diagenesis, and thus preserved more effectively in the rock record. Complex lipid structures are more favorably produced biologically making them unlikely to be formed abiotically (Flores et al., 2020). These factors make lipids ideal candidates as biosignatures.

Hopanoids are pentacyclic lipids that assist in regulating cellular membrane fluidity produced by bacteria (Ourisson et al., 1979). About 10% of bacteria are capable of producing hopanoids, and their complex structure challenges their polymerization via random abiotic processes (Ourisson and Albrecht, 1992). Hopanoids, which are estimated to constitute up to 0.1% of the total extractable organic content of all sediments (Ourisson and Albrecht, 1992), are highly abundant in biologically derived materials. On Earth, hopanoids have been found in kerogenous shale dating back to 2.7 Ga deposited in a marine continental shelf (Brocks et al., 1999). Hopanoids, sometimes referred to as geohopanoids in the geologic record, are resistant to diagenetic degradation making them well-preserved in the rock record, although the exact cause for this resistance is uncertain (Inglis et al., 2018; Ourisson and Albrecht, 1992). Thus, hopanoids may represent high fidelity biosignatures. Hopanoids share a complex backbone structure and cellular functionality with cholesterol (Figure 1), making cholesterol a useful (and more readily available) proxy for hopanoids. Hopanoids also share a strikingly similar structure with betulinic acid (Figure 1), a molecule often found in tree barks making betulinic acid a useful structural analog for hopanoids.

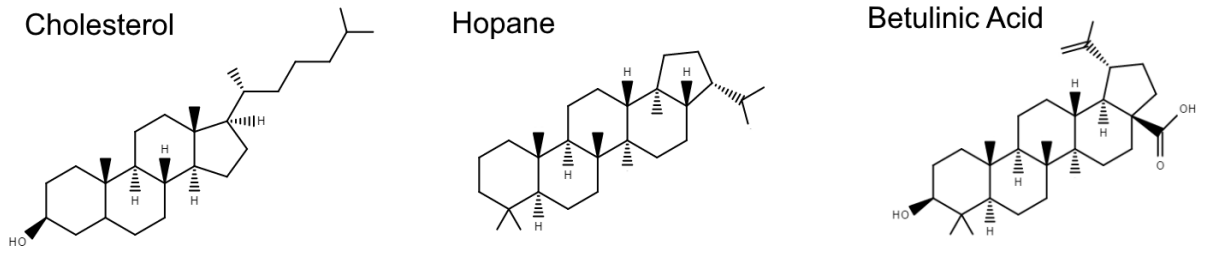

Figure 1: The chemical structure for three potential biosignatures: cholesterol serves to regulate membrane fluidity in mammals, hopane serves as the backbone structure for all hopanoids, and betulinic acid is a structural analog for hopanoids often found in tree bark.

The first goal of this study is to characterize subsurface mineralogy in a Mars analog lacustrine environment and compare this mineralogy to results collected using analogous commercial instrumentation in-situ at Gale crater on Mars. Understanding mineralogy from an analog site is important for informing on processes occurring on other planetary bodies. Mineralogy is one indicator for how comparable the geologic context and subsequent sedimentary processing of the analog site is to Mars, and this can be characterized using x-ray diffraction (XRD), a technique

currently in use by the Curiosity rover. It is hypothesized that the sediments at Lake Sandvatn will be a comparable mineralogical analog site for Gale crater because both are sourced from basaltic terrains, and Lake Sandvatn may be undergoing early diagenetic processes that would further develop a more similar composition to Mars; therefore, samples at Lake Sandvatn are expected to share the majority of their mineralogy with samples analyzed by CheMin on Mars. Secondly, the effects of mineralogy on the detectability of two lipids will be explored with LDMS using mineral references and a subset of Mars analog samples from Lake Sandvatn. Mineralogy may have an effect on the adsorption of organic molecules due to differences in crystal structure and chemistry; surface and interlayer properties; and crystallite size. Understanding the effects of mineralogy on the detectability of two lipids is important for choosing geologic targets for analysis during spaceflight and quantifying potential limitations on life detection.

2. Methods

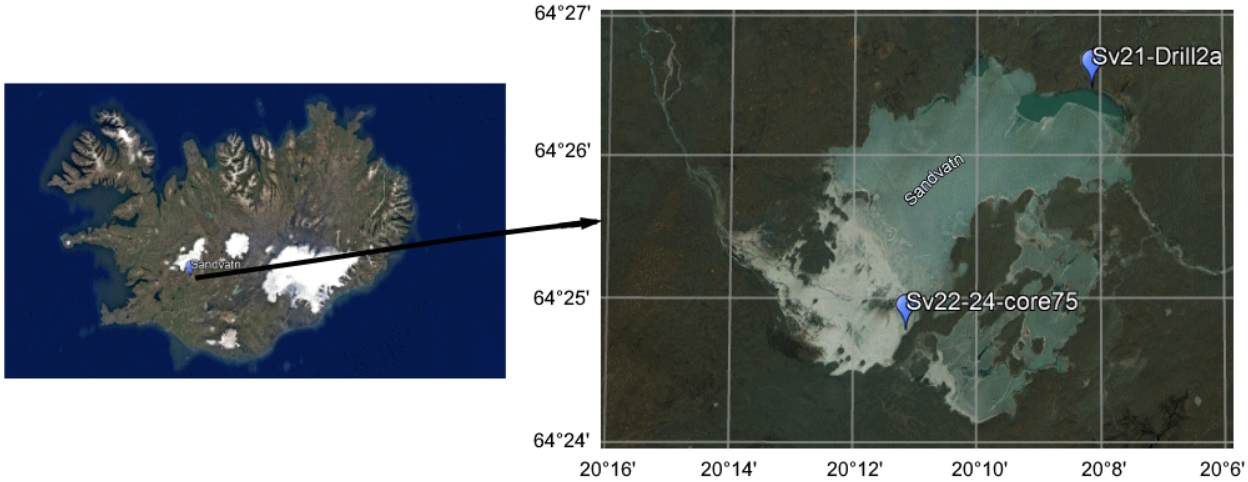

Figure 2: (Left) Aerial map of Iceland with the location of Lake Sandvatn marked by a blue pin. (Right) Aerial image of Lake Sandvatn with locations noted of drill cores collected by DIGMARS. SV22-24-core75 is used in this study. (Source: Google Earth)

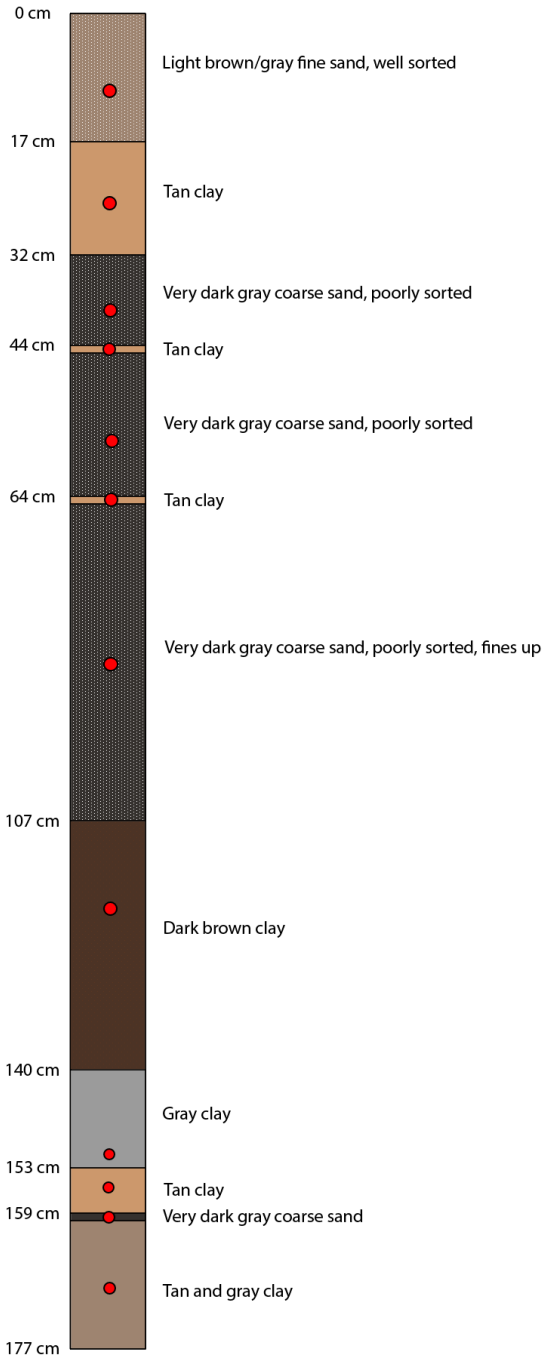

Figure 3: Schematic diagram of SV22-24-core75 with descriptions. Subsampling locations are identified with red dots (N=12).

2.1 Analog Samples

In addition to spaceflight exploration, Mars can be studied using analog environments on Earth. Analog environments share similar characteristics to the location (e.g. planetary body) of interest. Iceland and Hawaii are common martian analogs given they are two locations on Earth with subaerial basalt like Mars instead of the more common granitic and felsic terrains that makes up much of the Earth's accessible crust. Additionally, analog sites with colder climates can be more comparable to the conditions on Mars potentially producing more analogous geochemistry and surface processes that are temperature dependent. Analog studies allow for direct human exploration, cost-effective observation, and provide a reference frame for observations on other planetary bodies. This strategy was invoked for this project, and the analog site for this study is Lake Sandvatn in southwest Iceland. Iceland is primarily basaltic in composition and the climate is colder than other analog environments used for Mars such as Hawaii. Lake Sandvatn and the surrounding region encompass a range of depositional environments including deltaic, lacustrine, and fluvial (Thorpe et al., 2022).

Sediment samples were collected during the Digging Iceland Geology for Mars Analog Research Science (DIGMARS) 2022 field campaign to Lake Sandvatn in southwest Iceland (see Figure 2). One of the collected drill cores from the field campaign was SV22-24-core75, which was the primary focus of this study for drawing mineralogical comparisons to Mars. This core was collected in the shallow waters of Lake Sandvatn using a floating drill rig (see Figure S1). The core was sealed in the field and shipped back to NASA Goddard Space Flight Center (GSFC) where upon arrival it was stored in a freezer at -20°C. The drill core was collected in a cleaned aluminum container which was cut open using a metal nibbler, a tool which cut open the core by removing a thin (a few mm wide) section while introducing minimal aluminum debris into the core. The contents were transferred into a cleaned PVC pipe covered with ultra-high vacuum aluminum foil. From there, the exposed surface layer was scraped off with a bench scraper to remove vertical smearing of the layers on the exterior from the collection of the drill core, and subsamples were collected in a clean environment using lab coats, gloves, masks, and eyewear. Subsampled sediments were collected in two cleaned glass vials, one dedicated for future XRD measurements, and the other for laser desorption mass spectrometry (details provided below). All tools were rinsed after each use with ethanol to avoid organic contamination as well as cross contamination between subsamples.

2.2 Mineralogy and XRD

A method onboard the Curiosity rover working to understand the past environment of Mars is XRD. The CheMin instrument on board the Curiosity rover collects XRD patterns, and the team uses this data to quantify modal mineralogy based on the crystalline mineralogical structures and full pattern fitting techniques. The rover collects samples about two cm deep using a drill core in order to avoid alteration that may have occurred on the surface (Blake et al., 2012). XRD is a technique that characterizes the modal mineralogy by weight percent of powdered rock samples based on the structure of the constituent minerals. X-rays are aimed at the sample and the diffraction angles of the X-rays diffracted from the sample are measured. The product is a pattern where individual peaks indicate the diffraction angles produced by the d-spacings of the crystal lattice planes for minerals within the sample (see Figure S2); peak intensities provide insight into the abundance of each observed phase. This pattern can be used to quantify modal mineralogy

using Rietveld refinement techniques, an approach employed in this study using the Jade software package (Materials Data Inc.). For more quantitative mineralogy, an internal standard can be used. For these analyses, samples were doped with corundum, ~20% by weight, to be used as an internal standard.

Lake Sandvatn subsamples were prepped for XRD by measuring out approximately one gram of sediment, then grinding the sediments down to silt size and smaller (i.e., <= 63 microns) using a mortar and pestle lubricated with ethanol. After the ethanol dried, the sediments were added to a micronizing mill container with agate beads. They were milled for 10 minutes to produce < 10 micron grains, resulting in an approximately uniform grain size distribution and allowing for representative reflections from minerals in an "infinitely" thick sample. The sediment fines were front-loaded into powder specimen holders. All XRD analyses were completed at NASA Johnson Space Center using a Rigaku MiniFlex 600 with a Co-K_α radiation source and a DeTex detector. Scans were completed over a 5 to 70 2θ diffraction angle range with a 0.02 2θ step size, and 0.5-second dwell time per step. Using MDI Jade, a Rietveld refinement was completed on each XRD pattern; the program determined the uncertainty for each mineral phase based on the fit of the refinement to the pattern. Uncertainty in the refinements is calculated by Jade by examining the difference between the fit and raw data and individual peaks for each mineral. Uncertainty was further constrained by repeating the refinements without inputting a defined value for the internal standard (20 wt.% corundum). To enable a comparative analysis with the techniques used by CheMin onboard the Curiosity rover, several patterns from Lake Sandvatn were also analyzed using the FullPat Program (Chipera and Bish, 2002); details on the distinctions from these calibration techniques can be found in the Supplemental Material.

Mineralogical data from select sites along Curiosity's traverse within Gale crater were collected from the Open Data Repository CheMin database. A total of 35 samples, sourced from a variety of depositional environments, have thus far been collected along Curiosity's route, and analyzed by CheMin (as determined from multiple sources (Morrison et al., 2018; Rampe et al., 2020; Thorpe et al., 2022). These sample analyses were filtered to only include samples derived from lacustrine, fluvial, or deltaic, excluding aeolian environments and significantly diagenetically altered samples for the best comparison to Lake Sandvatn.

After filtering by depositional environment, 17 sample measurements remained. There was a total of 36 unique phases in these filtered samples, including amorphous silica, clays, and crystalline phases identified by CheMin. The full dataset used can be found in Supplemental Materials (see Table S1). To further classify the data, the mineralogy of each sample is broken into ten mineral groups/categories: Plagioclase, K-Spar, Pyroxene, Olivine, Fe and Ti Hydroxides and Oxides, Silica, Sulfates and Chlorides and Phosphates, Carbonates, Clays, and Amorphous (including opaline). Shared or overlapping mineralogy was calculated by comparing the mineralogy in the ten categories of each Lake Sandvatn sample to each CheMin sample. The sample with a lower value for modal % in each mineral category defined the percent overlap for that mineral group (i.e. if Icelandic sample SV22-24-core75 at 28 cm depth had 20% plagioclase and martian sample John Klein had 40% plagioclase, the percent overlap is 20%). The percent overlap for each mineral category was added together to determine the total overlap between each CheMin sample and Lake Sandvatn sample.

In order to understand the amorphous material present in the samples from Lake Sandvatn, X-ray fluorescence (XRF) data for major element geochemistry was collected at Washington State University. Data was collected using a Rigaku 3370 XRF Spectrometer with calibrations using basaltic USGS standards (i.e., BHVO-2). Full details about data collection can be found in Johnson, Hooper, and Conrey (1999). The percentage of amorphous material, composition of crystalline material, and bulk major element geochemistry can be used to calculate the geochemical composition of the amorphous material using a mass balance approach. This was completed using the bulk XRF data and XRD data for SV22-24-core75 samples. First crystalline geochemistry was approximated using the results from XRD. Then the crystalline geochemistry was weighted by the percent of crystalline material in the sample and subtracted from the bulk geochemistry. This value was normalized to the percent of amorphous material in the sample which resulted in the geochemistry of the amorphous material.

Analog	Relevance to Mars	Sample number	Citation
Three Sisters, OR	Cold	N = 20	(Rampe et al., 2022)
Tecopa Basin, CA	Volcanic, Lacustrine	N = 12	(Martin et al., 2020)
Hawaiian Analog Quarry	Basaltic	N = 8	(Edison et al., 2021)
Columbia River Basalt, ID	Cold, Basaltic	N = 11	(Thorpe and Hurowitz, 2020)
Hvalfjodour, Iceland	Cold, Basaltic	N = 10	(Ehlmann et al., 2012)

Table 1: List of analog sites used to provide further context for Lake Sandvatn.

XRD data were compiled from five alternative sites previously described as basaltic terrains and/or martian analog environments in order to provide further context for Lake Sandvatn as an analog site. These publications were selected based on sample number (e.g., statistical value), data availability (e.g., mineralogy and geochemistry), and sufficient analog site description. The five other analog sites shared the same climate, environment, or basaltic terrain that Lake Sandvatn did with Mars. They include Three Sisters, Tecopa Basin, Hawaii, Columbia River, and Iceland (Table 1).

2.3 LDMS and Organics

An analytical method that will be used on future missions to understand habitability and search for chemical signs of life on Mars is laser desorption mass spectrometry (LDMS), a spatially resolved imaging technique used to characterize abundances and distributions of organic and inorganic materials simultaneously with minimal sample destruction. A pulsed laser source enables rapid desorption and ionization of organic analytes, avoiding combustion and molecular degradation of organic compounds embedded in oxidative samples. The ESA ExoMars mission set to fly to Mars in 2028 (Clery, 2022) will deploy an LDMS instrument named the Mars Organic Molecule

Analyzer (MOMA) to Oxia Planum. The goal of MOMA is to characterize the organic material in the martian subsurface down to 2 m depth (Goesmann et al., 2017), where prospective biosignatures may be shielded at depth from incoming galactic and cosmic rays (Atri, 2020) and preserved from oxidative breakdown by oxychlorine species (Glavin et al., 2013). Additionally, the Dragonfly Mass Spectrometer (DraMS) will apply LDMS for the measurement of organic chemistry onboard the Dragonfly mission to Titan which will launch in 2027 (Grubisic et al., 2021).

LDMS analyses were completed using a Thermo Fisher Scientific Q Exactive (QE) Orbitrap™ Mass Spectrometer with a pulsed laser source and custom sample chamber and ion inlet system sub-atmospheric pressure (6-7 torr) designed and installed by Spectroglyph, LLC. The output of the laser (200 uJ of 266 nm wavelength) works well for the analysis of aromatic organics as carbon ring structures absorb deep UV wavelengths. All analyses scanned across a mass range of m/z 50 - 750, detecting positively charged ions with a mass resolving power of $m/\Delta m$ = 70,000 (Full Width Half Maximum at m/z 100).

2.3.1 Baseline Measurements

Because the sample plate in the custom QE sample chamber is positioned vertically, sediments were adhered to double sided carbon tape. The carbon tape would be present in all subsequent analyses, so the first analyses completed were background measurements of the carbon tape (approximately 1500 scans) to identify major peaks that may infiltrate further analyses.

Both mineral references, and samples from Lake Sandvatn were analyzed via LDMS by creating sediment mounts with carbon tape. Each sediment mount was prepared using gloves, eyewear, and masks in order to prevent unnecessary organic contamination. Tools used to handle the sediment mounts were cleaned with acetone before and after each use.

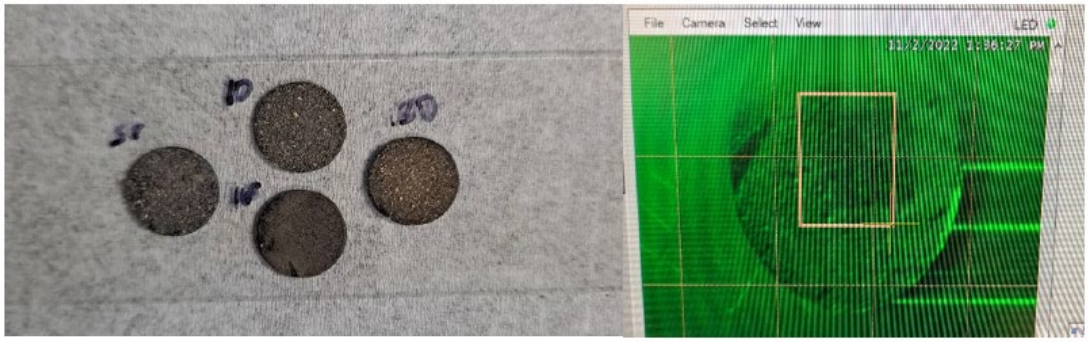

Figure 4: (Left) Nine mm sediment mounts adhered to the glass plate. (Right) Sediment mount as viewed from the instrument's navigation camera. The orange box represents an analyzed area.

The mineral references used were montmorillonite, augite, labradorite, and dunite, which has greater than 90% olivine (Table 2). These references were selected as proxies to the common mineralogy observed in Lake Sandvatn and Gale crater. Augite and labradorite match the pyroxene and plagioclase components of the Lake Sandvatn mineralogy, respectively. The montmorillonite, labradorite, and dunite were already in powdered form, while the augite sample was powdered using a mortar and pestle following the same process described above.

Name	Locality
Dunite (USGS DTS-2b 0390)	Twin Sisters, WA
Augite (Eisco Labs)	Unknown
Labradorite	Oregon
Montmorillonite (Swy-2)	Crook County, WY

Table 2: List of mineral references used in this study.

Baseline measurements for each mineral reference mounted on carbon tape were completed (3x runs of approximately 2000 scans) in order to constrain diagnostic inorganic peaks representing each phase. Then baseline characterization of powdered samples from Lake Sandvatn were completed with two analyses, the first approximately 1000 scans long in a small area using 0.02 mm step size, and the second approximately 2000 scans long in a large area using 0.075 mm step size for higher and lower resolution characterization given the heterogeneity of the samples.

2.3.2 Doped Analysis

The purpose of using LDMS in this study was to simulate experiments completed by future spaceflight missions while measuring organic and inorganic signals simultaneously. To test the effects of mineralogy on lipid detectability mineral references were doped with potential biosignatures, to provide clear results for the individual influence of minerals on these potential biosignature's detectability. While hopanoids would be the ideal target organic, cholesterol was used since it was readily available, affordable, and serves as a functional analog to hopanoids in regulating cellular membrane fluidity (Sáenz et al., 2015). Additionally, for further testing, betulinic acid, pentacyclic triterpene that shares a nearly identical chemical structure to hopanoids was also used. The use of both these potential biosignatures allowed for the characterization of a functional analog and structural analog for hopanoids.

For the last round of LDMS analyses, sediments (mineral references and Lake Sandvatn samples) were doped with either cholesterol, a functional analog to hopanoids, or betulinic acid, a structural analog to hopanoids, using a slurry method similar to that used for testing of the ExoMars MOMA prototype instruments (e.g., Arevalo et al., 2015; Li et al., 2017). Organic solutions were prepared by dissolving powdered target lipids, specifically cholesterol (Sigma Aldrich PN; >99% or betulinic acid (Sigma Aldrich PN; >90% purity), in methanol to reach a desired concentration. After creating an organic solution with the desired molarity, approximately 0.5 cc of dry powdered mineral reference was measured in a microcentrifuge tube. Then the prepared solution was added to the sediments in a microcentrifuge tube and set to dry. After drying, the samples were poured out onto a sterile petri dish where they were mounted to carbon tape using the method described above and analyzed on the QE.

Solutions of cholesterol were prepared over three separate days to create an extended sensitivity curve. Full details on the preparation of solutions can be found in Supplemental Materials. One

mount of a single concentration doped onto a single mineral reference was created for each mineral reference (four mounts per concentration). Each mount was then analyzed in three areas for roughly 1000 scans, or 0.4 mm^2, each with a blank analysis of the mineral reference for 200 scans in between each doped analysis.

Analyses for betulinic acid were completed in a single lab day. A solution of 0.001M betulinic acid in methanol was prepared using 0.0053 g of betulinic acid powder and 10 mL of methanol. This concentration was chosen because it is near the maximum solubility of betulinic acid in methanol at room temperature (Cheng et al., 2011). One doped mount was created for each mineral reference. Since there was only one concentration, analyses were 2000 scans long with 200 scans in between on blank mineral references.

LDMS data were processed using Thermo Scientific FreeStyle™ software. This program outputs individual spectra of intensity vs m/z for each scan collected during analysis. Data were quantified using a signal-to-noise ratio (S/N). The signal is calculated as the height, or maximum intensity, of an individual m/z peak, and noise is calculated as "peak-to-peak" noise, which is the difference between the maximum and minimum of noise values surrounding the peak. A S/N for a 1000 scan analysis is calculated by taking the mean of the intensity of an individual peak across all scans and this is divided by an averaged noise value, which is the mean noise divided by the square root of the number of scans. Further data processing was completed using MATLAB for doped peak identification and calculating uncertainty per analysis (as the root mean square of the S/N ratio across the analysis).

3. Results – Lake Sandvatn and Other Analogs

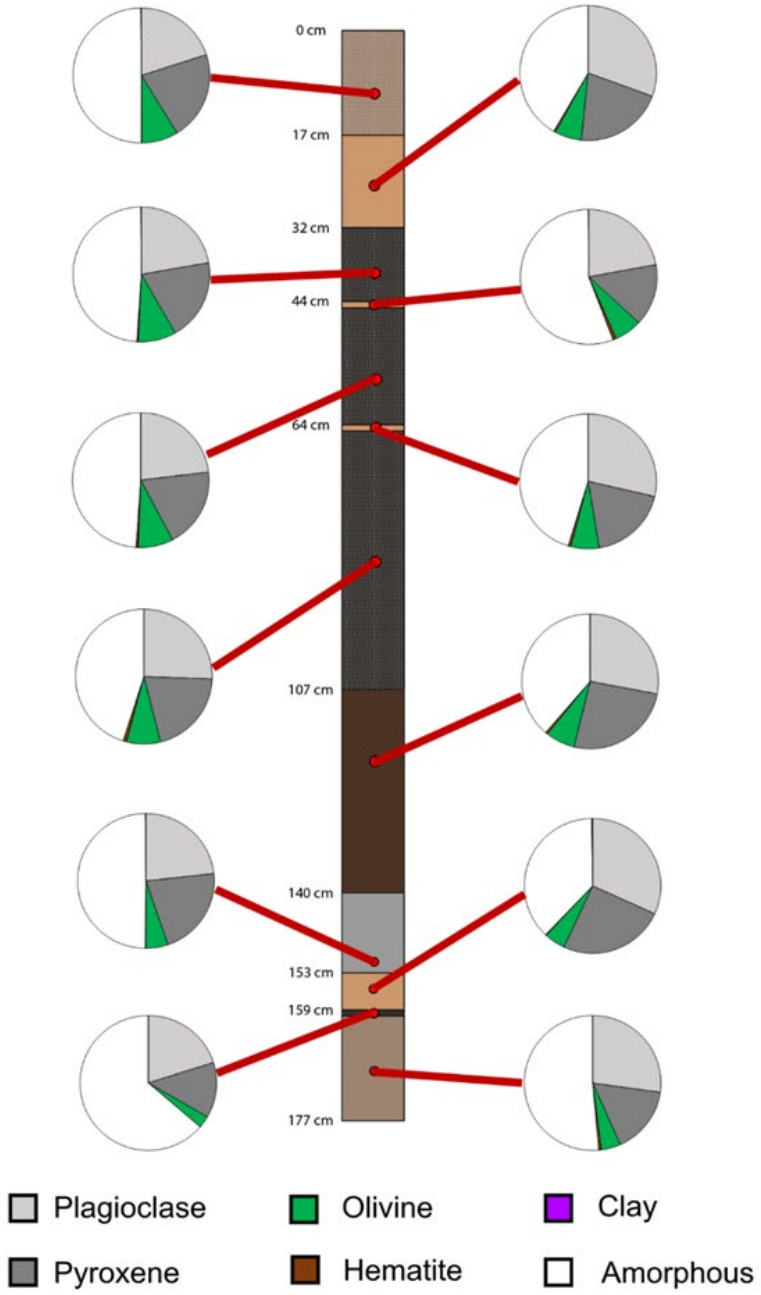

Figure 5: Modal mineralogy for each SV22-24-core75 subsample. Individual pie charts point to their respective subsampling locations with a dark red line. While clay is present in some of these samples, it is too low to be seen on the pie charts. Legend for mineralogy can be found at the bottom of the figure. This key includes amorphous material (white).

3.1 Mineralogy

3.1.1 SV22-24-core75

The SV22-24-core75 subsamples contain plagioclase, pyroxene, olivine, amorphous material, hematite, and clay (see Table S2 for full composition). Amorphous material often comprises the majority of the samples, and between the twelve samples there is a range of 38 to 64 % amorphous material. In the crystalline material of this core, plagioclase is often the most abundant mineral with a range of 40 to 56 % followed by 34 to 43 % pyroxene, 8 to 18 % olivine, up to 2 % hematite, and up to 0.4% nontronite. Notably, samples from this drill core have broad shallow peaks at around 8 2θ that correlate well with nontronite; however, because these peaks were so broad, they were not easy to fit during the refinement.

The drill core contains a range of grain sizes, grain shapes, and colors (Figure 3). Overall, the core coarsens upwards as the depositional environment changed. The base of the core is composed of clays of various colors with occasional, thin sand layers. The top half of the core contains more coarse sediments, mostly sand with thin layers of clay.

3.1.2 Gale Crater, Mars Samples

The samples analyzed by CheMin have mineralogies consistent with a basaltic provenance. The selected samples (believed to be lacustrine, fluvial, and/or deltaic in origin), have mostly basaltic minerals including plagioclase, pyroxene, and olivine. The filtered samples are mostly mudstone and sandstone lithologies. All samples have plagioclase in a range from 33 to 63 % in the crystalline component of the samples. Samples also have pyroxene between 2 and 32 %, and about half of the samples have no olivine. CheMin analysis also shows significant amounts of amorphous material in many samples from 20 to 53 %. Some samples also contain clay minerals in concentrations up to 34 %. Other minerals present include tridymite, hematite, magnetite, and others.

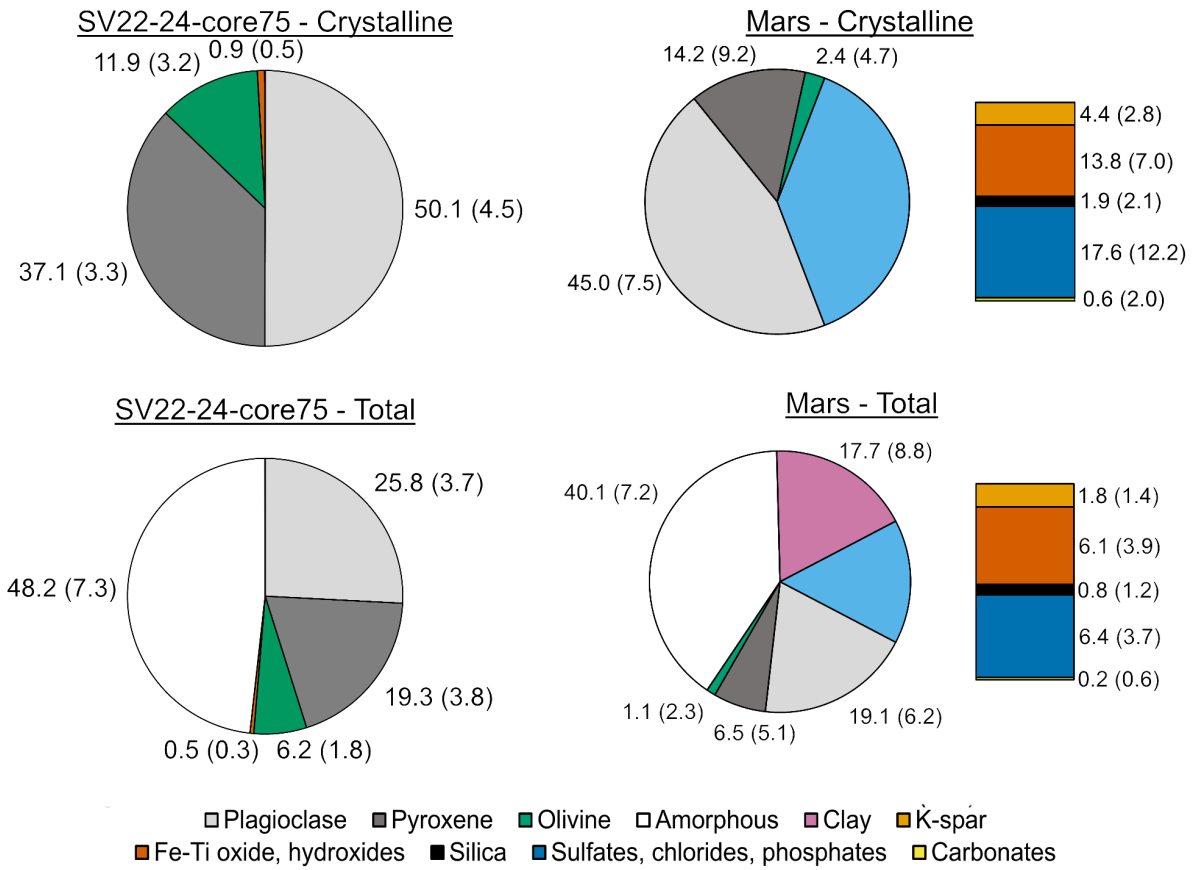

Figure 6: Average mineralogy for the Lake Sandvatn drill core and samples analyzed by CheMin (Mars). The top pie charts included only well-defined crystalline material (removing amorphous material and clays), and the bottom includes all phases present in the samples. The drill cores have notably higher amorphous material on average than martian samples, and there is a wider diversity of minerals present on Mars.

3.1.3 Analog Mineralogy

The five alternative analog sites have a range of mineralogies. Three Sisters, OR, as described by Rampe et al. (2022), is comprised mostly of plagioclase followed by amorphous material, pyroxene, olivine, quartz, and Fe-Ti oxides. Samples from Tecopa Basin, CA, as described by Martin et al. (2020), have a range of provenance and mineralogies. This includes amorphous material, plagioclase, carbonates, quartz, K-feldspar, and some amphiboles. Similarly, samples from Hvalfjodour Iceland described in Ehlmann et al. (2012) also have a wide range of mineralogies including plagioclase, pyroxene, clay, and zeolites, and did not report amorphous material. The quarry and analog sites presented in Edison et al. (2021) also have plagioclase, pyroxene, and olivine like many other sites, but the cristobalite, and ilmenite are unique. Finally, samples from the Columbia River Basalt watershed from Thorpe et al. (2021) include plagioclase, pyroxene, K-feldspar, quartz, clays, olivine, small amounts of Fe-Ti oxides and micas, and amorphous material.

3.2 Comparable Mineralogy

The SV22-24-core75 samples have mineralogy comparable to samples analyzed by CheMin. When comparing the entire mineralogy including amorphous material, all SV22-24-core75 samples have at least 50% comparable mineralogy with all 17 of the CheMin samples. This number is slightly lower when comparing exclusively the crystalline component. Subsamples from 47 cm and 168 cm have the greatest comparable total mineralogies on average with samples from CheMin, averaging 66 and 67%, respectively. Subsamples from 118 cm and 147 cm have the lowest comparable total mineralogy on average with samples from CheMin, averaging 63 and 64%, respectively. Overall, the range of comparable mineralogy between SV22-24-core75 samples and CheMin mostly falls between 50 and 80%. On average, Mojave2, a CheMin sample, had the greatest comparable mineralogy with samples from SV22-24-core75 and with samples from Lake Sandvatn overall, averaging more than about 77% comparable total and crystalline mineralogy. Conversely, Glen Etive 1 from CheMin have the lowest comparable mineralogy to samples from Lake Sandvatn averaging 51 and 46% comparable total and crystalline mineralogy respectively.

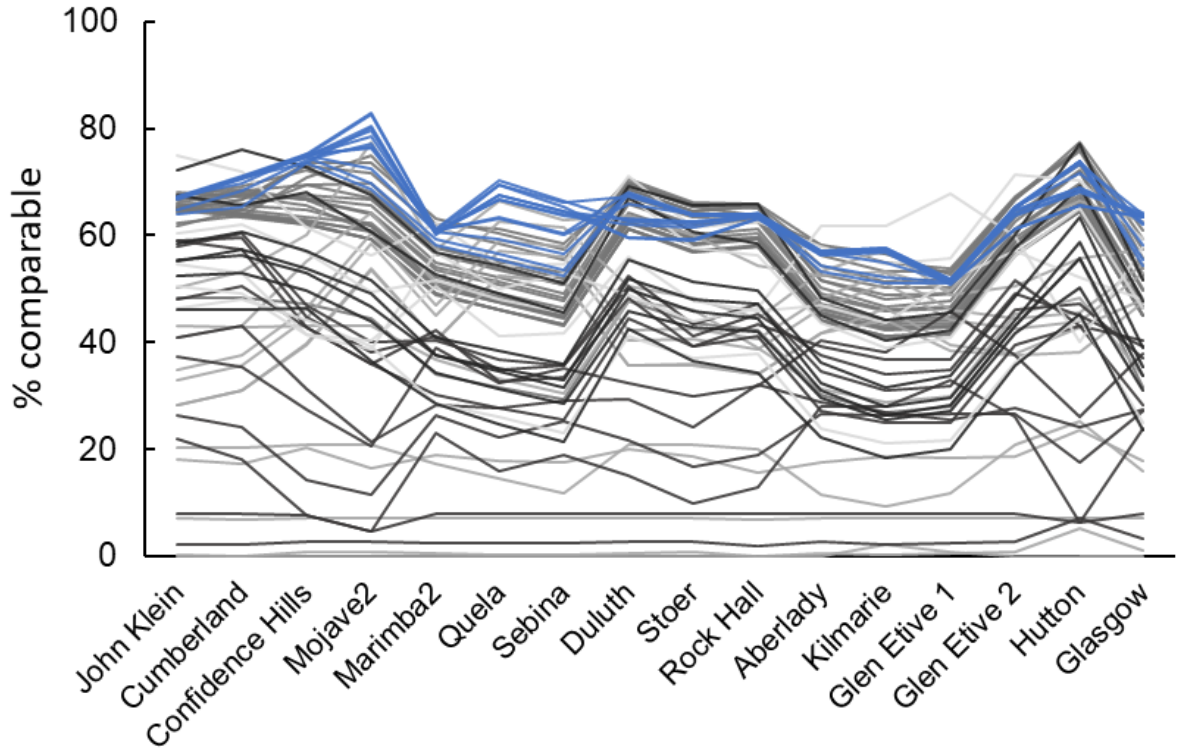

Figure 7: Comparable mineralogy between samples from each analog site and Gale crater. Each line represents a different sample, and each point on the line represents the comparisons between that analog sample and a sample from Mars (the x-axis). Lines are 50% transparent in order to see overlapping comparisons.

A comparison of the mineralogy of the other analog sites to Gale crater can be seen in Figure 7. Of the other analog sites, samples from Three Sisters had the greatest consistency across samples in comparability to CheMin samples. Additionally, Three Sisters had the highest comparable mineralogy of the five other analog sites, although samples from Three Sisters were still less

comparable than samples from Lake Sandvatn. Samples from Tecopa Basin had a wide range of comparable total mineralogy from as low as 7 to up to 77%. Hvalfjodour and Columbia River Basalt samples also had similarly wide ranges. Across all analog sites samples including Lake Sandvatn, on average samples had greater total comparable mineralogy than crystalline comparable mineralogy due to the inclusion of amorphous material. Samples from Hvalfjdour showed the opposite trend, where comparable mineralogy was higher when examining the crystalline material. Overall, samples from Lake Sandvatn demonstrated higher comparable mineralogy and greater consistency across samples than other analog sites.

3.3 Bulk Geochemistry

This characterization of amorphous material at Lake Sandvatn shows some difference with the bulk geochemistry of the samples (see Table S3 for full bulk geochemistry and Table S4 for calculated amorphous geochemistry). Notably, the amorphous material has a lower percentage of SiO_2 and greater percentage of FeO and Al_2O_3, while most other oxides had percentages within 10% of the bulk geochemistry. The results are plotted in Figure 8 on a Si-Al-Fe ternary diagram, elements that often dominate the geochemistry of amorphous materials. Amorphous endmembers and clays are label for further context. The geochemistry of the amorphous material does not correlate with any endmember, but rather plots near the center of the plot indicating the composition is likely a mixture.

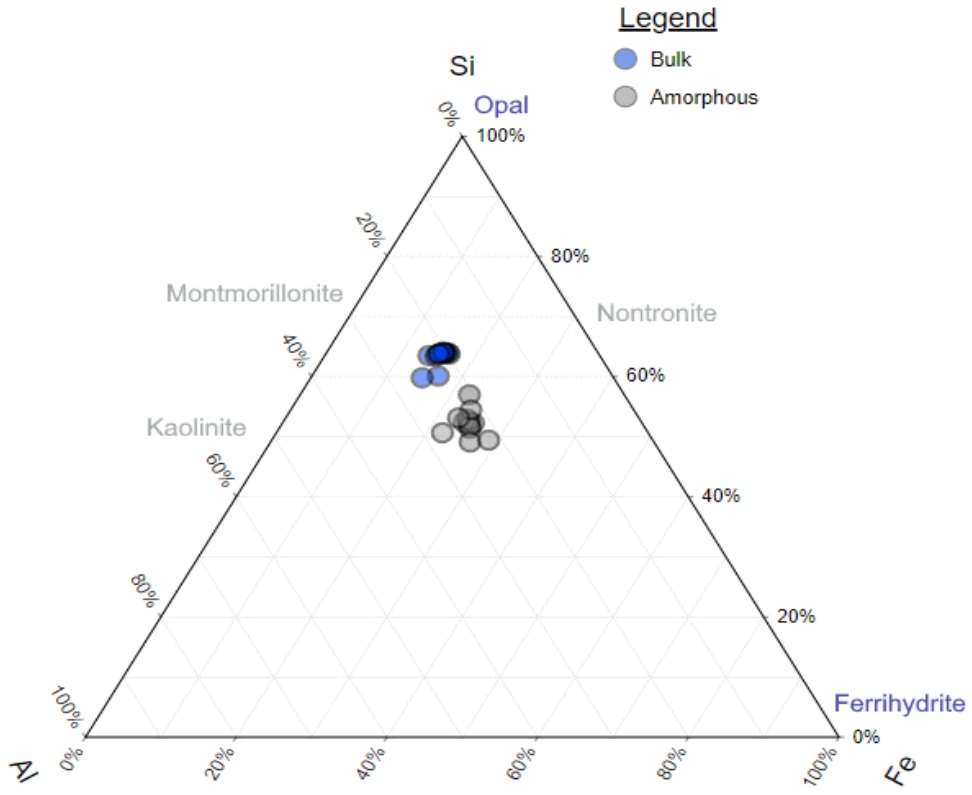

Figure 8: Si-Al-Fe ternary plot for geochemistry of Lake Sandvatn bulk and amorphous. Amorphous endmembers (blue) and crystalline clays (gray) also labeled for comparison. Ternary diagram can be used to inform on weathering and chemical evolution.

4. Lipids and LDMS

Carbon tape was used in all experiments as the medium for mounting sediments to the glass plate. Before analyzing the sediment samples, the carbon tape was characterized via LDMS to identify peaks characteristic of the medium, effectively representing a "blank" analysis for subsequent measurements. The carbon tape has a major peak at m/z 171.093, an organic likely derived from the tape adhesive.

4.1 Doped Mineral References

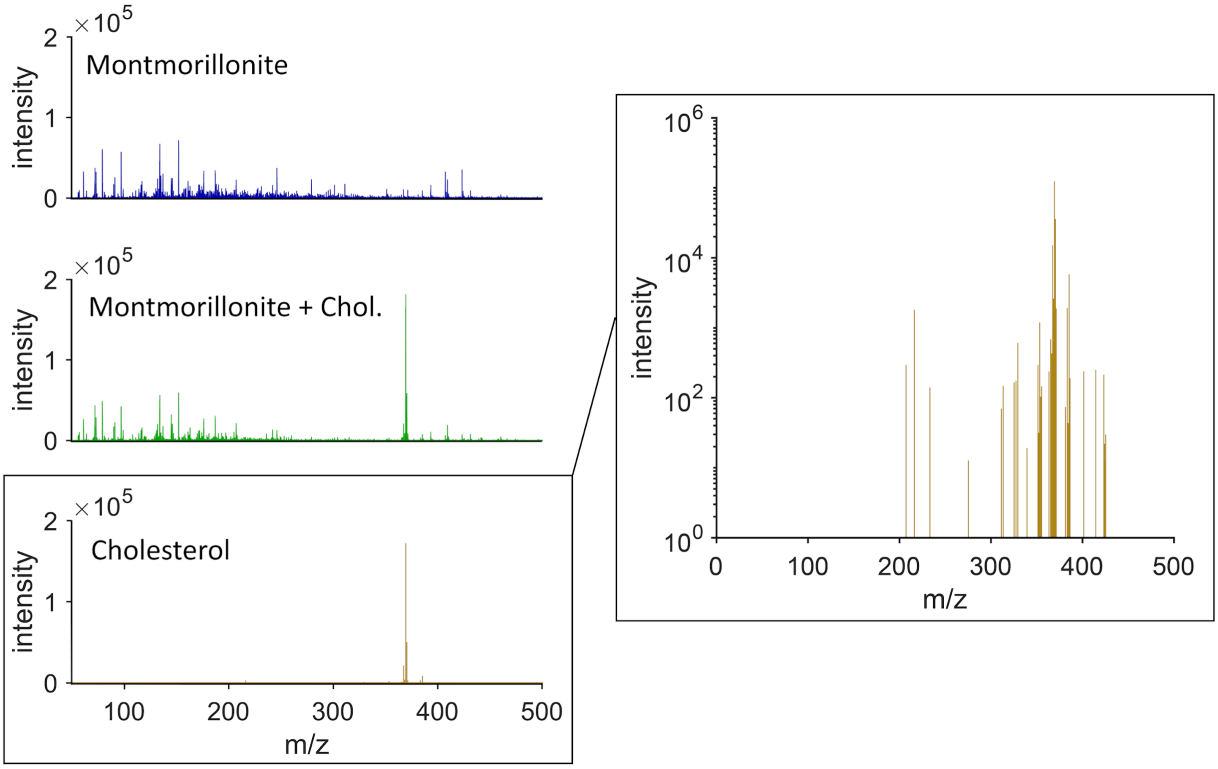

Figure 9: LDMS spectra for a neat mineral standard, doped mineral standard, and new peaks produced in the doped analysis. The new peaks are also plotted on a log scale for improved visibility.

In order to distinguish molecular signatures representative of the organic analyte during the analysis of doped sediments, spectral peaks sourced from the carbon tape and mineral matrices were identified and compared to the doped spectra by using MATLAB; peaks derived from the organic analyte were then manually confirmed. Across all doped analyses, a total of 74 discrete new peaks spanning between 200 and 500 m/z were determined to represent cholesterol (see Figure

9). During cholesterol doped analysis, the highest intensity peak is consistently observed at 369.35 m/z, a diagnostic fragment reflecting a protonated and dehydrated cholesterol molecular ion (M^++H–H_2O). For betulinic acid, a total of 9 discrete peaks spanning 390 and 600 m/z are observed in doped analyses. Unlike cholesterol, the peaks produced by betulinic acid routinely have low S/N ratios and are only present above S/N = 3, considered background, during analysis with montmorillonite.

By measuring S/N of cholesterol peaks at different concentrations, a sensitivity curve was created for each mineral reference (Figure 10). These results show a decrease in S/N of 369 with a decrease in molarity, however, the trend is different for each mineral reference. At higher molarities (0.0025 – 0.01 M), the S/N of 369 on montmorillonite is greater, up to an order of magnitude. The dunite sensitivity curve has the most non-linear trend of the four mineral references. At higher molarities, the S/N of 369 plateaus around 100. However, below 0.001 M the S/N is below the background during all analyses. Labradorite and augite both have relatively linear sensitivity curves compared to dunite and montmorillonite. At 0.01 M, augite has an average of 457 S/N, which decreases linearly to 2 S/N at 0.000025 M. Similarly, labradorite starts with an S/N of 377 at 0.01 M, and linearly decreases to S/N of 1 at 0.000025 M. All mineral references are below the background of S/N = 3 by 0.000025 M.

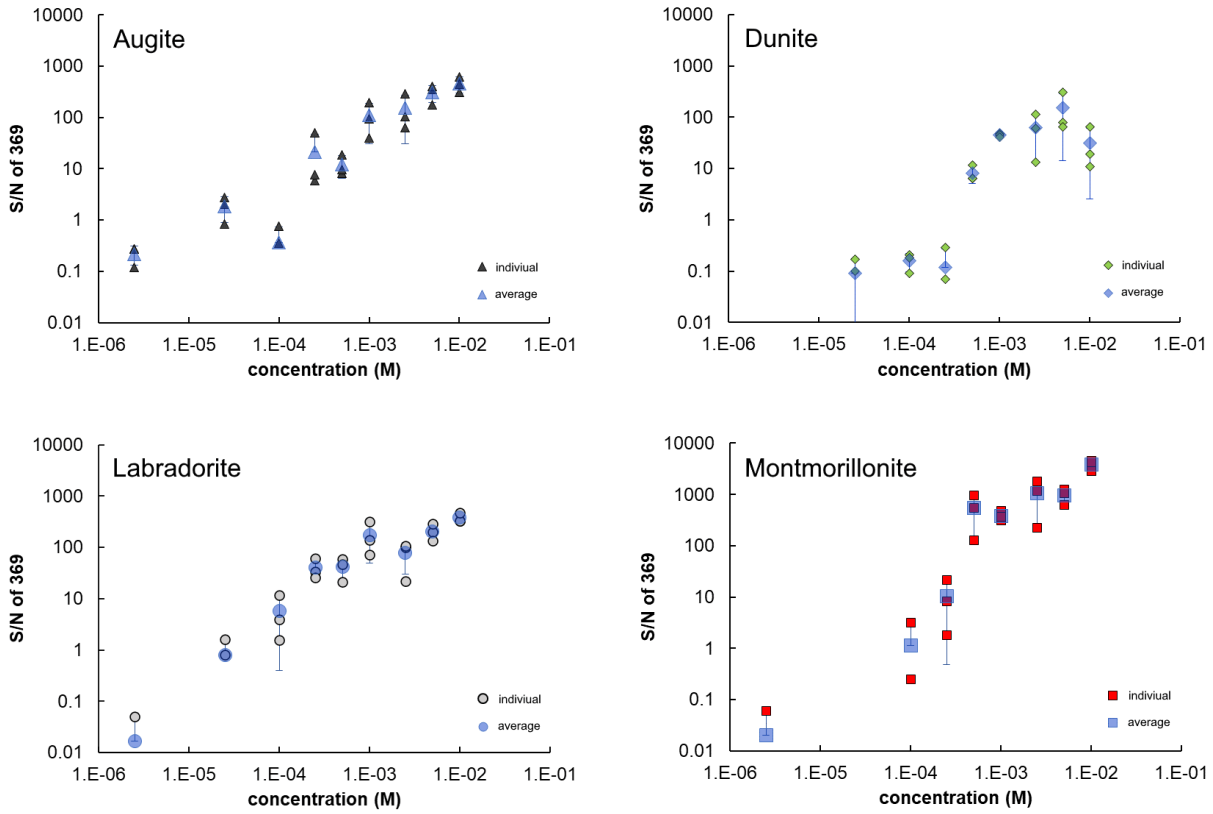

Figure 10: Sensitivity curves for each mineral reference analyzed. Three data points were collected at each concentration, although sometimes the S/N ratio was 0 resulting in some missing points on the log-log scale. Light blue transparent points are the average of the three analyses at each concentration, and error bars are the standard deviation.

Based on the average S/N ratios from each analysis, detection limits can be inferred. For augite and montmorillonite, the concentration at the background of 3 is between 0.00025 M and 0.0001 M, considering propagated uncertainties in the model regression. The detection limit for cholesterol on dunite is slightly higher, between 0.0005 M and 0.00025 M, though fewer data are used to define the curve due to the lack of linearity in sensitivity. Finally, cholesterol on labradorite has the lowest detectable concentration, which falls between 0.0001 M and 0.000025 M.

Sensitivity curves for the multicomponent analog samples were also calculated using the average S/N ratios across three analyses (Figure 11). The two analog samples used were from a depth of 147 cm and 157 cm because they had the lowest and highest amorphous material, respectively. Both these samples have S/N ratios over 100 S/N at the highest molarity, 0.01 M, and decrease to below the S/N of 3 by 0.0001 M. On average, these curves are lower than any of the mineral references alone.

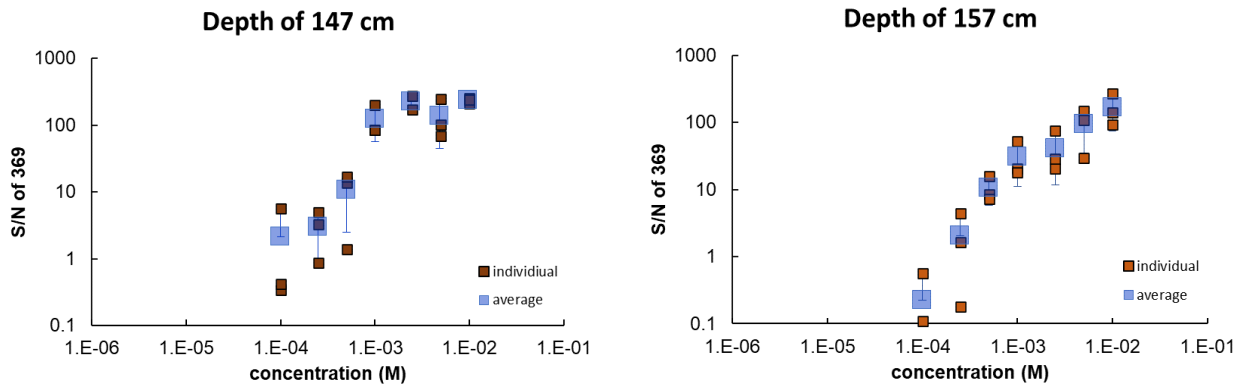

Figure 10: Sensitivity curves for two samples from Lake Sandvatn. These sensitivity curves are prepared in the same manner as the mineral references above.

5 Discussion

5.1 Mineralogy and Depositional Environments at Lake Sandvatn

The drill core from Lake Sandvatn records many years of changing depositional environments. This core was collected approximately 40 m from the present-day shoreline, and the shortest width across the lake near this drill core is approximately 1300 m. While the core was collected offshore, it was still relatively close to the shoreline allowing for the deposition of the coarser sand sediment layer seen at the very top of the core. Over time, the shape of the shoreline and lake varied, as inferred from the clay layers likely deposited in a deeper lacustrine environment. Coarser sediments present in the drill core could also be a product of inputs from the nearby delta of the lake. As the top layer of the core is more poorly sorted than other sandy layers in the core, it is likely the top layer had some input from the delta, whereas the deeper sand layers may be more associated with the lake shoreline. Of the samples used in this study, Lake Sandvatn has the most comparable mineralogy to lacustrine samples from Pahrump Hills on Mars (Mojave2 and

Confidence Hills). Conversely, Lake Sandvatn is least comparable to the fluvio-lacustrine samples from the Glen Torridon region.

Of the analog sites explored in this study, Lake Sandvatn is the most mineralogically similar to Gale crater. The major component that differs between Lake Sandvatn and Gale crater is the clay fraction. There is some evidence that clay may be forming in the subsurface of Lake Sandvatn, but they appear to be poorly crystalline. The XRD patterns for SV22-24-core75 do show a very shallow and broad peak at 9.5 degrees 2θ indicating the presence of clay minerals. This shallow peak most closely matches a peak produced by nontronite, although montmorillonite is another potential candidate. The broadness of this peak was difficult to fit during refinements due to the narrower peaks used in the fit, leaving little to no crystalline clay present in the refinements. However, the presence of this peak indicates clays are present in the sample and furthermore may still be developing into more crystalline phases, leaving some percentage of clay in the x-ray amorphous material. The sediments from Lake Sandvatn are still relatively young compared to samples from Mars meaning diagenetic processes have not had as much time to occur. The colder climate of Iceland would also slow the formation of clay minerals. Additionally, Thorpe et al. (2022), references lower modal % of amorphous material for samples collected at the surface of Lake Sandvatn, and higher modal % of amorphous material for samples in the subsurface. Because clay formation can be a diagenetic process (e.g., neoformed or transformed clay minerals), it is possible that the formation of poorly crystalline clay minerals is contributing to an increase in amorphous material in the subsurface. Furthermore, evidence from the mass balance calculated geochemistry of the amorphous material (Figure 8) at Lake Sandvatn points to an amorphous mixture. This could be a combination of opal and ferrihydrite and/or juvenile clays including nontronite and montmorillonite.

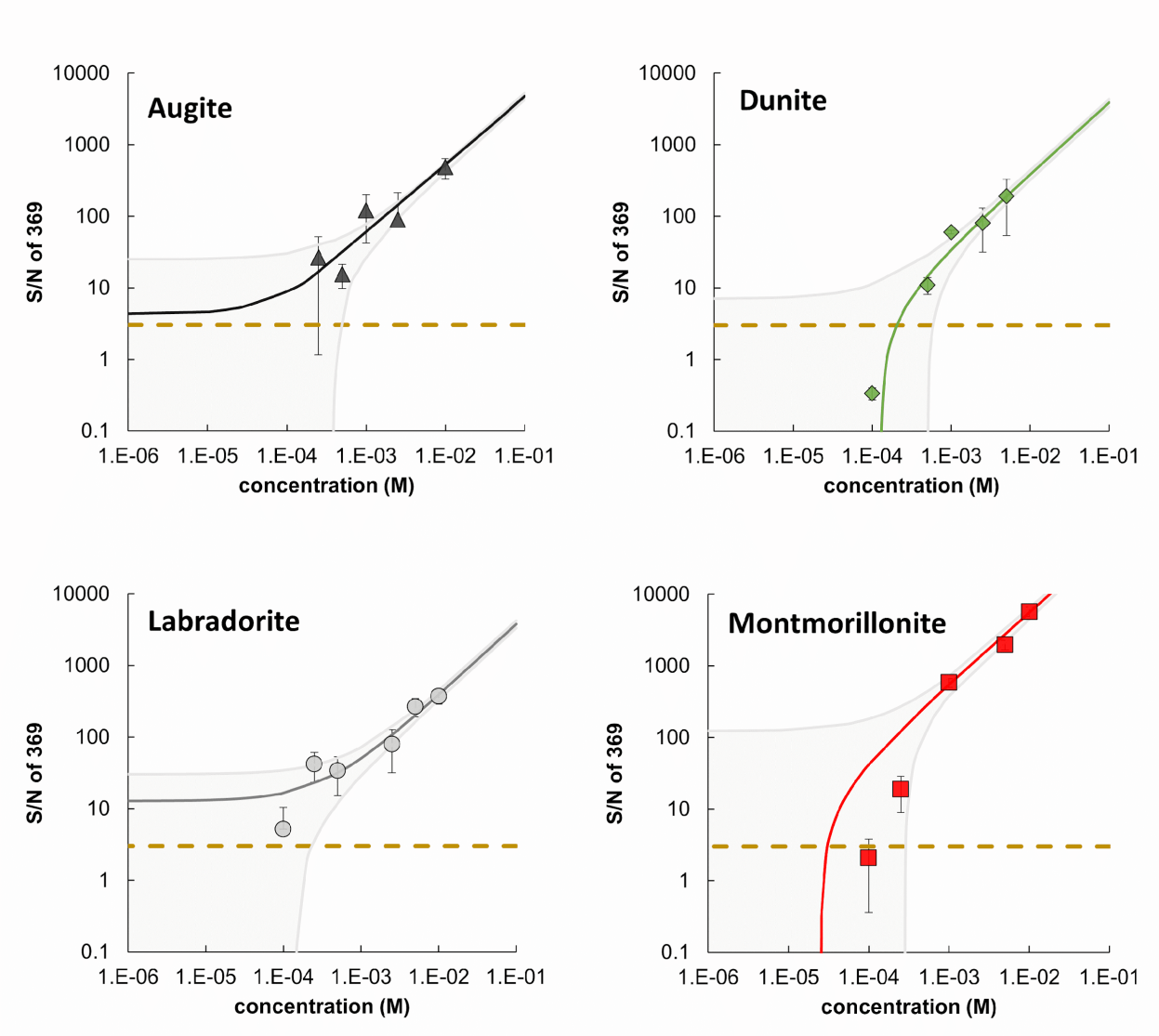

Figure 12: Robust linear regressions (solid colored lines) with 95 % confidence interval shaded in light gray. Outliers identified by residuals greater than the median absolute deviation of the residuals, and data points below S/N 3 (outside analytical uncertainty), are not included in the linear regression analyses. A S/N of 3 is also highlighted with a dark yellow dashed line. Details on these regressions can be found in the Supplemental Material

5.2 LDMS Sensitivity Curves

Robust linear regression analysis was applied to the sensitivity curve for each doped mineral reference described previously (see Figure 9). The trendline for each curve enables extrapolation to the inferred detection limit of cholesterol for each mineral reference (Figure 11). Based on these sensitivity curve regressions, dunite is characterized by the highest detection limit at 0.00021 M +/- 0.0004 M. In contrast, the lowest detection limit observed was facilitated by montmorillonite

at 0.00003 M +/- 0.00026. Because the best fit regressions for augite and labradorite do not cross S/N of 3, only a range for the limit of detection can be determined. For augite, the range for the limit of detection is between 0 and 0.00046 M, and for labradorite the range for the limit of detection of cholesterol is between 0 and 0.00024 M.

Regressions were also completed using the natural analog samples derived from Lake Sandvatn. For the sample from a depth of 147 cm, the limit of detection of cholesterol is 0.000083 M +/- 0.00031. Similarly, for the sample from a depth of 157 cm, the mean limit of detection of cholesterol is 0.0001 M +/- 0.00028. For both the raw data and regressions, the analog samples on average had lower S/N ratios than the augite, montmorillonite, and labradorite mineral references, but similar values with dunite. The sample from 147 cm has 37 % amorphous material, and the sample from 157 cm has the most amorphous material at 67 %. Considering the most significant difference between the mineral references and analog samples is the presence of amorphous material, this may be a contributing factor to the decrease in S/N relative to the mineral references. This is further supported by 147 cm having less amorphous material than 157 cm and 147 cm having a higher S/N ratio on average.

5.3 Controls on Organic Detection via LDMS

Organic adsorption to mineral surfaces can be affected by a wide range of environmental parameters, including mineral surface pH, molecule polarity, and molecule structure (Kleber et al., 2021). Once bonded to the mineral surface, there are a multitude of mechanisms that can influence the detectability of those organics, including the physicochemical properties of the matrix (in this case the mineral) to the analytical performance of the instrumentation which are quickly reviewed here.

The UV absorption behavior of every mineral varies; phases with a greater absorbance of 266 nm will couple more effectively with the incident photon beam, leading to more efficient thermal desorption of organics. While there is not a single repository of absorbance spectra for all four of mineral references under the same analytical conditions, reflectance spectra can be used to infer the percentage of incident light absorbed as a function of wavelength. Cloutis et al., (2008) measured the reflectance spectra for various compositions of plagioclase, olivine, clay, and pyroxene. Whereas montmorillonite, augite, and olivine all have around 5% reflectance at the 266 nm wavelength, plagioclase is higher at 12-15 % reflectance. From these results, it can be inferred that plagioclase would have the lowest % absorbance (and transmittance) while the remaining three minerals would have roughly the same % absorbance. If % absorbance of the laser wavelength is a signifignat control on the detectability of organics on mineral surfaces, than it would be expected that plagioclase would have the lowest S/N ratios of the four mineral references studied. However, as seen in Figure 12, the S/N ratios for plagioclase were not lower than olivine (dunite). The S/N ratios of cholesterol on olivine may have been influenced by space charge effects, where a significant influx of ions prevents all ions from reaching the detector. Evidence for space charge effects during analysis of dunite is supported by the total intensity measured in each scan being an order of magnitude higher than the total intensities measured for other minerals. Alternatively, another potential influence could be mineral absorption of organic molecules; clay minerals are capable of swelling to accommodate an influx of organic cations, and during the doping processing, swelling was observed on montmorillonite.

5.4 Other Analytical Considerations

Given that the lowest mass-to-charge ratio that the QE can measure is m/z 50, many major elements cannot be measured making it difficult to determine which minerals the laser is hitting on each shot in a mixed sample. In the Lake Sandvatn samples, peaks for iron, copper, rubidium, and manganese have been identified in one or more baseline sediment spectra. These elements can potentially be used to inform on which mineral each laser shot is hitting, however, because the laser spot size is 0.015 mm in diameter, and many grains within the powdered samples may be smaller than this, identifying the mineralogy at each laser shot would be very difficult. Unfortunately, this placed limitations on the use of spectral imaging since the target for individual shots could be more than one grain at a time.

Betulinic acid and cholesterol both have relatively low absorbance at 266 nm wavelength, the wavelength of the laser utilized on both MOMA and DraMS (Goesmann et al., 2017; Grubisic et al., 2021). Based on the similarity in structure between betulinic acid and hopanoids and the inability to detect betulinic acid on several common minerals present on the martian surface, detecting hopanoids may be a challenge. An important difference between the spaceflight and commercial instruments used in this study is the pressures at which the sample chamber and detector operate at. These differences in pressures will result in differences in thermodynamics of the system resulting in variation in particle ionization between the spaceflight and commercial instruments. Additionally, samples analyzed by MOMA will be laid flat in a sample tray, whereas the sample analyzed in this study had to be mounted to carbon tape since the sample plate is upright.

While using mineral references can be used to infer the potential effects minerals from Lake Sandvatn and on Mars would have on select lipid detectability, there are some limitations to this experiment. First, a potentially important variable that was not controlled in these experiments was grain size. Samples were all powdered in order to attempt to reduce potential effects from grain size, but there is still a wide range of grain sizes present in these samples. On average, larger grain sizes could constitute a lower total surface area concentration, since fewer grains could be packed onto the tape. Conversely smaller grains could result in a higher total surface area concentration because more grains will be packed onto the tape. Another potential limitation is variations in major and trace element geochemistry between the mineral references and analog and Mars samples. Finally, the mechanisms behind mineral effects on detectability are still poorly understood and are actively being researched. There will likely be important controllable variables for future mineral effect studies that are unable to be identified and controlled at this time.

6 Conclusions

This study explored comparable mineralogy in a Mars analog environment and its effects on the detectability of potential biosignatures. The results showed the sediments at Lake Sandvatn are very comparable with Gale crater mineralogically as both have a suite of basaltic minerals and amorphous material. Relative to other locations that have been used as analog sites, Lake Sandvatn is most comparable to the lacustrine, fluvial, and deltaic environments on Mars. Additionally the minerals present at Lake Sandvatn and on Mars including plagioclase, pyroxene, olivine, and clay have varying effects on the detectability of betulinic acid and cholesterol, potential biosignatures. The structural analog for hopanoids, betulinic acid, was below detection limits for most minerals

tested, despite using a solution near the maximum solubility of betulinic acid. An important next step in understanding mineralogical effects on biosignature detectability would be placing a more restrictive constraint on grain size (i.e. by sieving samples) in order to eliminate grain size as a potential variable. Additionally, completing experiments using minerals collected at the analog site rather than mineral references would reduce differences in geochemistry.

Acknowledgements

I'd like to start by thanking my three advisors: Dr. Arevalo, Dr. Thorpe, and Ashley Hanna for their support and guidance throughout my senior thesis. Ashley Hanna provided me with an excelled foundation in biology and organics and I am so grateful for her time and patience with me as I learned. She also showed me how to prepare organic solutions and sediment mounts for analysis during my project. Dr. Thorpe helped me learn so much about sedimentary geochemistry, Mars analog science, and XRD. He always supported my scientific curiosity, and I am so thankful for the opportunity to expand on work from the DIGMARS project. Dr. Arevalo introduced me to the realm of spaceflight instrumentation and helped support all aspects of this project from end to end. I am so thankful for all the work my advisors have done.

I would also like to thank Dr. Elizabeth Rampe for completing XRD analyses at NASA JSC and for thoughtful discussion on our XRD results. And I would like to thank my boyfriend James Boggs for his programming in Rust for extraction of raw data from QE files, and for assistance with MATLAB code for data processing.

Finally, I would like to thank Dr. Piccoli. His support on this project through regular scientific discussions has helped me think outside-of-the-box. He has also done an amazing job coordinating the senior thesis program that helped make this research experience so meaningful to me.

7. References

Atri, D., 2020. Investigating the biological potential of galactic cosmic ray-induced radiation-driven chemical disequilibrium in the Martian subsurface environment. Sci Rep 10, 11646. https://doi.org/10.1038/s41598-020-68715-7

Baker, V.R., 2006. Geomorphological Evidence for Water on Mars. Elements 2, 139–143. https://doi.org/10.2113/gselements.2.3.139

Blake, D., Vaniman, D., Achilles, C., Anderson, R., Bish, D., Bristow, T., Chen, C., Chipera, S., Crisp, J., Des Marais, D., Downs, R.T., Farmer, J., Feldman, S., Fonda, M., Gailhanou, M., Ma, H., Ming, D.W., Morris, R.V., Sarrazin, P., Stolper, E., Treiman, A., Yen, A., 2012. Characterization and Calibration of the CheMin Mineralogical Instrument on Mars Science Laboratory. Space Sci Rev 170, 341–399. https://doi.org/10.1007/s11214-012-9905-1

Brocks, J.J., Logan, G.A., Buick, R., Summons, R.E., 1999. Archean Molecular Fossils and the Early Rise of Eukaryotes. Science 285, 1033–1036. https://doi.org/10.1126/science.285.5430.1033

Cheng, Y., Shao, Y., Yan, W., 2011. Solubilities of Betulinic Acid in Thirteen Organic Solvents at Different Temperatures. J. Chem. Eng. Data 56, 4587–4591. https://doi.org/10.1021/je200531k

Chipera, S.J., Bish, D.L., 2002. *FULLPAT*: a full-pattern quantitative analysis program for X-ray powder diffraction using measured and calculated patterns. J Appl Crystallogr 35, 744–749. https://doi.org/10.1107/S0021889802017405

Clery, D., 2022. Europe tries to save Mars rover after split with Russia. Science 376, 124–124. https://doi.org/10.1126/science.abq3938

Cloutis, E.A., McCormack, K.A., Bell, J.F., Hendrix, A.R., Bailey, D.T., Craig, M.A., Mertzman, S.A., Robinson, M.S., Riner, M.A., 2008. Ultraviolet spectral reflectance properties of common planetary minerals. Icarus 197, 321–347. https://doi.org/10.1016/j.icarus.2008.04.018

Committee on the Planetary Science and Astrobiology Decadal Survey, Space Studies Board, Division on Engineering and Physical Sciences, National Academies of Sciences, Engineering, and Medicine, 2022. Origins, Worlds, and Life: A Decadal Strategy for Planetary Science and Astrobiology 2023-2032. National Academies Press, Washington, D.C. https://doi.org/10.17226/26522

Edison, K., Andersen, C., Harford, K., Tokunaga, J., Romo, R., 2021. The Effects of Mineral Abundances on Mechanical and Structural Properties of Sintered Hawaiian Basalt Aggregate: Implications for Lunar/Mars ISRU Applications, in: Earth and Space 2021. Presented at the 17th Biennial International Conference on Engineering, Science, Construction, and Operations in Challenging Environments, American Society of Civil Engineers, Virtual Conference, pp. 818–831. https://doi.org/10.1061/9780784483374.076

Ehlmann, B.L., Bish, D.L., Ruff, S.W., Mustard, J.F., 2012. Mineralogy and chemistry of altered Icelandic basalts: Application to clay mineral detection and understanding aqueous environments on Mars: CLAY MINERAL DETECTION, ICELANDIC BASALT. J. Geophys. Res. 117, n/a-n/a. https://doi.org/10.1029/2012JE004156

Ehlmann, B.L., Mustard, J.F., Murchie, S.L., Bibring, J.-P., Meunier, A., Fraeman, A.A., Langevin, Y., 2011. Subsurface water and clay mineral formation during the early history of Mars. Nature 479, 53–60. https://doi.org/10.1038/nature10582

Fairén, A.G., 2010. A cold and wet Mars. Icarus 208, 165–175. https://doi.org/10.1016/j.icarus.2010.01.006

Flores, J., White, B.M., Brea, R.J., Baskin, J.M., Devaraj, N.K., 2020. Lipids: chemical tools for their synthesis, modification, and analysis. Chem. Soc. Rev. 49, 4602–4614. https://doi.org/10.1039/D0CS00154F

Glavin, D.P., Freissinet, C., Miller, K.E., Eigenbrode, J.L., Brunner, A.E., Buch, A., Sutter, B., Archer, P.D., Atreya, S.K., Brinckerhoff, W.B., Cabane, M., Coll, P., Conrad, P.G., Coscia, D., Dworkin, J.P., Franz, H.B., Grotzinger, J.P., Leshin, L.A., Martin, M.G., McKay, C., Ming, D.W., Navarro-González, R., Pavlov, A., Steele, A., Summons, R.E., Szopa, C., Teinturier, S., Mahaffy, P.R., 2013. Evidence for perchlorates and the origin of chlorinated hydrocarbons detected by SAM at the Rocknest aeolian deposit in Gale Crater: EVIDENCE FOR PERCHLORATES AT ROCKNEST. J. Geophys. Res. Planets 118, 1955–1973. https://doi.org/10.1002/jgre.20144

Goesmann, F., Brinckerhoff, W.B., Raulin, F., Goetz, W., Danell, R.M., Getty, S.A., Siljeström, S., Mißbach, H., Steininger, H., Arevalo, R.D., Buch, A., Freissinet, C., Grubisic, A., Meierhenrich, U.J., Pinnick, V.T., Stalport, F., Szopa, C., Vago, J.L., Lindner, R., Schulte, M.D., Brucato, J.R., Glavin, D.P., Grand, N., Li, X., van Amerom, F.H.W., the MOMA Science Team, 2017. The Mars Organic Molecule Analyzer (MOMA) Instrument: Characterization of Organic Material in Martian Sediments. Astrobiology 17, 655–685. https://doi.org/10.1089/ast.2016.1551

Grotzinger, J.P., Gupta, S., Malin, M.C., Rubin, D.M., Schieber, J., Siebach, K., Sumner, D.Y., Stack, K.M., Vasavada, A.R., Arvidson, R.E., Calef, F., Edgar, L., Fischer, W.F., Grant, J.A., Griffes, J., Kah, L.C., Lamb, M.P., Lewis, K.W., Mangold, N., Minitti, M.E., Palucis, M., Rice, M., Williams, R.M.E., Yingst, R.A., Blake, D., Blaney, D., Conrad, P., Crisp, J., Dietrich, W.E., Dromart, G., Edgett, K.S., Ewing, R.C., Gellert, R., Hurowitz, J.A., Kocurek, G., Mahaffy, P., McBride, M.J., McLennan, S.M., Mischna, M., Ming, D., Milliken, R., Newsom, H., Oehler, D., Parker, T.J., Vaniman, D., Wiens, R.C., Wilson, S.A., 2015. Deposition, exhumation, and paleoclimate of an ancient lake deposit, Gale crater, Mars. Science 350, aac7575. https://doi.org/10.1126/science.aac7575

Grubisic, A., Trainer, M.G., Li, X., Brinckerhoff, W.B., van Amerom, F.H., Danell, R.M., Costa, J.T., Castillo, M., Kaplan, D., Zacny, K., 2021. Laser Desorption Mass Spectrometry at Saturn's moon Titan. International Journal of Mass Spectrometry 470, 116707. https://doi.org/10.1016/j.ijms.2021.116707

Haberle, R.M., 1998. Early Mars Climate Models. J. Geophys. Res. 103, 28467–28479. https://doi.org/10.1029/98JE01396

Hubbard, G.S., Naderi, F.M., Garvin, J.B., Field, M., 2002. Following the Water, The New Program for Mars Exploration 14.

Inglis, G.N., Naafs, B.D.A., Zheng, Y., McClymont, E.L., Evershed, R.P., Pancost, R.D., 2018. Distributions of geohopanoids in peat: Implications for the use of hopanoid-based proxies in natural archives. Geochimica et Cosmochimica Acta 224, 249–261. https://doi.org/10.1016/j.gca.2017.12.029

Johnson, D.M., Hooper, P.R., Conrey, R.M., 1999. XRF Analysis of Rocks and Minerals for Major and Trace Elements on a Single Low Dilution Li-tetraborate Fused Bead 2.

Kleber, M., Bourg, I.C., Coward, E.K., Hansel, C.M., Myneni, S.C.B., Nunan, N., 2021. Dynamic interactions at the mineral–organic matter interface. Nat Rev Earth Environ 2, 402–421. https://doi.org/10.1038/s43017-021-00162-y

Li, X., Danell, R.M., Brinckerhoff, W.B., Pinnick, V.T., van Amerom, F., Arevalo, R.D., Getty, S.A., Mahaffy, P.R., Steininger, H., Goesmann, F., 2015. Detection of Trace Organics in Mars Analog Samples Containing Perchlorate by Laser Desorption/Ionization Mass Spectrometry. Astrobiology 15, 104–110. https://doi.org/10.1089/ast.2014.1203

Martin, P.E., Ehlmann, B.L., Thomas, N.H., Wiens, R.C., Hollis, J.J.R., Beegle, L.W., Bhartia, R., Clegg, S.M., Blaney, D.L., 2020. Studies of a Lacustrine-Volcanic Mars Analog Field Site With Mars-2020-Like Instruments. Earth and Space Science 7, e2019EA000720. https://doi.org/10.1029/2019EA000720

Morrison, S.M., Downs, R.T., Blake, D.F., Vaniman, D.T., Ming, D.W., Hazen, R.M., Treiman, A.H., Achilles, C.N., Yen, A.S., Morris, R.V., Rampe, E.B., Bristow, T.F., Chipera, S.J., Sarrazin, P.C., Gellert, R., Fendrich, K.V., Morookian, J.M., Farmer, J.D., Des Marais, D.J., Craig, P.I., 2018. Crystal chemistry of martian minerals from Bradbury Landing through Naukluft Plateau, Gale crater, Mars. American Mineralogist 103, 857–871. https://doi.org/10.2138/am-2018-6124

Orosei, R., Lauro, S.E., Pettinelli, E., Cicchetti, A., Coradini, M., Cosciotti, B., Di Paolo, F., Flamini, E., Mattei, E., Pajola, M., Soldovieri, F., Cartacci, M., Cassenti, F., Frigeri, A., Giuppi, S., Martufi, R., Masdea, A., Mitri, G., Nenna, C., Noschese, R., Restano, M., Seu, R., 2018. Radar evidence of subglacial liquid water on Mars. Science 361, 490–493. https://doi.org/10.1126/science.aar7268

Ourisson, G., Albrecht, P., 1992. Hopanoids. 1. Geohopanoids: the most abundant natural products on Earth? Acc. Chem. Res. 25, 398–402. https://doi.org/10.1021/ar00021a003

Ourisson, G., Albrecht, P., Rohmer, M., 1979. The Hopanoids: Paleochemistry and Biochemistry of a Group of Natural Products. Pure and Applied Chemistry 51, 709–729.

Pollack, J.B., Kasting, J.F., Richardson, S.M., Poliakoff, K., 1987. The case for a wet, warm climate on early Mars. Icarus 71, 203–224. https://doi.org/10.1016/0019-1035(87)90147-3

R. Arevalo, W. Brinckerhoff, F. van Amerom, R. Danell, V. Pinnick, Xiang Li, S. Getty, L. Hovmand, A. Grubisic, P. Mahaffy, F. Goesmann, H. Steininger, 2015. Design and demonstration of the Mars Organic Molecule Analyzer (MOMA) on the ExoMars 2018 rover, in: 2015 IEEE Aerospace Conference. Presented at the 2015 IEEE Aerospace Conference, pp. 1–11. https://doi.org/10.1109/AERO.2015.7119073

Rampe, E.B., Bristow, T.F., Morris, R.V., Morrison, S.M., Achilles, C.N., Ming, D.W., Vaniman, D.T., Blake, D.F., Tu, V.M., Chipera, S.J., Yen, A.S., Peretyazhko, T.S., Downs, R.T., Hazen, R.M., Treiman, A.H., Grotzinger, J.P., Castle, N., Craig, P.I., Des Marais, D.J., Thorpe, M.T., Walroth, R.C., Downs, G.W., Fraeman, A.A., Siebach, K.L., Gellert, R., Lafuente, B., McAdam, A.C., Meslin, P. -Y., Sutter, B., Salvatore, M.R., 2020. Mineralogy of Vera Rubin Ridge From the Mars Science Laboratory CheMin Instrument. J. Geophys. Res. Planets 125. https://doi.org/10.1029/2019JE006306

Rampe, E.B., Horgan, B.H.N., Smith, R.J., Scudder, N.A., Bamber, E.R., Rutledge, A.M., Christoffersen, R., 2022. A mineralogical study of glacial flour from Three Sisters, Oregon: An analog for a cold and icy early Mars. Earth and Planetary Science Letters 584, 117471. https://doi.org/10.1016/j.epsl.2022.117471

Sáenz, J.P., Grosser, D., Bradley, A.S., Lagny, T.J., Lavrynenko, O., Broda, M., Simons, K., 2015. Hopanoids as functional analogues of cholesterol in bacterial membranes. Proc. Natl. Acad. Sci. U.S.A. 112, 11971–11976. https://doi.org/10.1073/pnas.1515607112

Tarnas, J.D., Mustard, J.F., Sherwood Lollar, B., Stamenković, V., Cannon, K.M., Lorand, J.-P., Onstott, T.C., Michalski, J.R., Warr, O., Palumbo, A.M., Plesa, A.-C., 2021. Earth-like Habitable Environments in the Subsurface of Mars. Astrobiology 21, 741–756. https://doi.org/10.1089/ast.2020.2386

Team, R., 1997. Characterization of the Martian Surface Deposits by the Mars Pathfinder Rover, Sojourner. Science 278, 1765–1768. https://doi.org/10.1126/science.278.5344.1765

Thorpe, M., Rampe, E.B., Tamborski, J.J., Siebach, K.L., Putnam, A., Kovtun, R., Lynch, K.L., Leeb, D., Gundjonsson, G., Tu, V.M., Ewing, R.C., Bedford, C., 2022. Overview and Initial Results of DIGMARS: Digging Iceland Geology for Mars Analog Research Science. Presented at the 53rd Lunar and Planetary Science Conference, Houston, TX.

Thorpe, M.T., Bristow, T.F., Rampe, E.B., Tosca, N.J., Grotzinger, J.P., Bennett, K.A., Achilles, C.N., Blake, D.F., Chipera, S.J., Downs, G., Downs, R.T., Morrison, S.M., Tu, V., Castle, N., Craig, P., Marais, D.J.D., Hazen, R.M., Ming, D.W., Morris, R.V., Treiman, A.H., Vaniman, D.T., Yen, A.S., Vasavada, A.R., Dehouck, E., Bridges, J.C., Berger, J., McAdam, A., Peretyazhko, T., Siebach, K.L., Bryk, A.B., Fox, V.K., Fedo, C.M., 2022. Mars Science Laboratory CheMin Data From the Glen Torridon Region and the Significance of Lake-Groundwater Interactions in Interpreting Mineralogy and Sedimentary History. Journal of Geophysical Research: Planets 127, e2021JE007099. https://doi.org/10.1029/2021JE007099

Thorpe, M.T., Hurowitz, J.A., 2020. Unraveling sedimentary processes in fluvial sediments from two basalt dominated watersheds in northern Idaho, USA. Chemical Geology 550, 119673. https://doi.org/10.1016/j.chemgeo.2020.119673

Vago, J.L., Westall, F., Pasteur Instrument Teams, Landing S, Coates, A.J., Jaumann, R., Korablev, O., Ciarletti, V., Mitrofanov, I., Josset, J.-L., De Sanctis, M.C., Bibring, J.-P., Rull, F., Goesmann, F., Steininger, H., Goetz, W., Brinckerhoff, W., Szopa, C., Raulin, F., Westall, F., Edwards, H.G.M., Whyte, L.G., Fairén, A.G., Bibring, J.-P., Bridges, J., Hauber, E., Ori, G.G., Werner, S., Loizeau, D., Kuzmin, R.O., Williams, R.M.E., Flahaut, J., Forget, F., Vago, J.L., Rodionov, D., Korablev, O., Svedhem, H., Sefton-Nash, E., Kminek, G., Lorenzoni, L., Joudrier, L., Mikhailov, V., Zashchirinskiy, A., Alexashkin, S., Calantropio, F., Merlo, A., Poulakis, P., Witasse, O., Bayle, O., Bayón, S., Meierhenrich, U., Carter, J., García-Ruiz, J.M., Baglioni, P., Haldemann, A., Ball, A.J., Debus, A., Lindner, R., Haessig, F., Monteiro, D., Trautner, R., Voland, C., Rebeyre, P., Goulty, D., Didot, F., Durrant, S., Zekri, E., Koschny, D., Toni, A., Visentin, G., Zwick, M., van Winnendael, M., Azkarate, M., Carreau, C., the ExoMars Project Team, 2017. Habitability on Early Mars and the Search for Biosignatures with the ExoMars Rover. Astrobiology 17, 471–510. https://doi.org/10.1089/ast.2016.1533

Wordsworth, R.D., 2016. The Climate of Early Mars. Annu. Rev. Earth Planet. Sci. 44, 381–408. https://doi.org/10.1146/annurev-earth-060115-012355

Wray, J.J., 2013. Gale crater: the Mars Science Laboratory/Curiosity Rover Landing Site. International Journal of Astrobiology 12, 25–38. https://doi.org/10.1017/S1473550412000328

8. Supplemental Materials

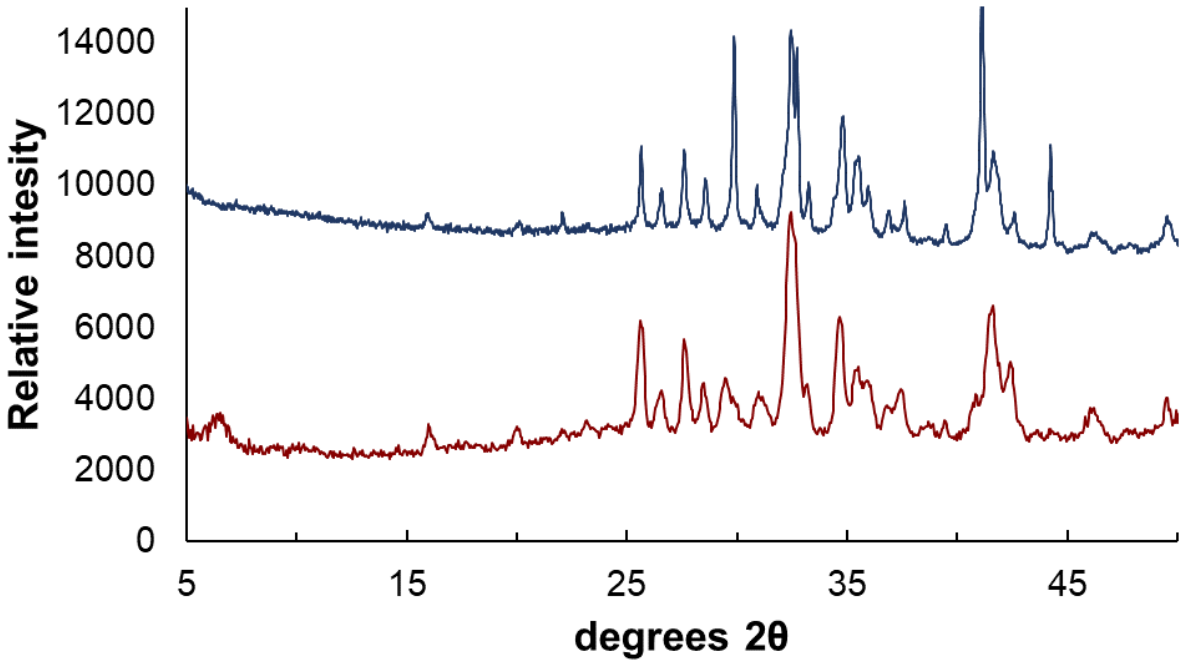

Figure S1: Examples of XRD patterns from Lake Sandvatn (top, blue) and Gale crater (bottom red) with adjusted relative intensities for comparison.

Figure S2: The floating drill rig used by the DIGMARS team to collect samples at Lake Sandvatn.

8.1 FullPat

In addition to MDI Jade, another program developed to quantify modal mineralogy is FullPat (Chipera and Bish, 2002). This program uses patterns of mineral standards analyzed using the same XRD instrument in order to fit a pattern. Ideally, standard patterns are collected on the same instrument used to measure XRD patterns of the samples, however, standards have not yet been measured on the XRD instrument used in this study. The pattern library used was the LANL library. FullPat was used in addition to MDI Jade to quantify the amorphous and clay abundance in samples analyzed by CheMin because these samples do not contain an internal standard. Because the samples analyzed in this study do have an internal standard, MDI Jade is the more appropriate program for quantifying modal mineral abundance. However, in an effort to remain somewhat analogous to the techniques used by CheMin, several patterns from Lake Sandvatn were also analyzed using FullPat to compare the amorphous and clay abundances from each program.

Unfortunately during the fitting process with FullPat, library patterns would not fully align with peaks present in the Lake Sandvatn sample. This is likely a product of using a library of reference patterns measured on a difference instrument. There is no library of patterns for the XRD instrument used in this study, so the FullPat analysis could not continue.

8.2 LDMS Sample Preparation

In between sample preparation steps, sediments derived from the SV22-24-core75 drill core were stored in a freezer at -20°C. When the samples were ready for analysis, they were ground using a mortar and pestle cleaned with acetone then ethanol to create a more uniform grain size < 63 um (silt sized and smaller). This protocol acted as an alternative to sieving, which could have changed the modal mineralogy of the samples given potential mineralogical grain size biases.

The first set of analyses focused on higher molarities. This started with 0.0391 g cholesterol dissolved in 10 mL of methanol to create a 0.01 M solution. Solutions of 0.005 M and 0.0025 M were created using a dilution series. The second set of analyses focused on exploring lower molarities by orders of magnitude. Similarly, this started with 0.0967 g of cholesterol dissolved in 100 mL of methanol to create a 0.0025 M solution. Then 0.00025 M, 0.000025 M and 0.0000025 M solutions were created using dilution series. Finally, the third set of analyses worked to fill in some more uncertain areas on the sensitivity curve. These solutions were prepared starting with 0.0383 g of cholesterol in 100 mL of methanol for a 0.001 M solution, then concentrations of 0.0005M, and 0.0001M were made using a dilution series. The final total over three days was 9 different cholesterol concentration solutions analyzed.

8.3 Regression Techniques

Robust regression is a unique method of linear regression. It examines the slopes between every pair (n*(n-1)/2) of data points and takes the median as the slope of a linear regression line. This method is useful for datasets susceptible to outliers. A robust regression is less influenced by outliers than other methods. Solved with the following equations:

$$m = Med\left(\frac{y_j - y_i}{x_j - x_i}\right)$$

$$b = \bar{y} - m\bar{x}$$

Linear regressions are likely the most appropriate fit for the dataset collected in this study, however, they do not always follow a linear trend. Sensitivity curves may plateau at their highest and lowest points as a product of analytical mechanisms creating a sigmoidal curve. For example, space charge effects could result in some of the plateauing of the highest S/N points produced in the dunite sensitivity curve. When examining the sum of intensities of all masses measured during dunite analysis, it was on average an order of magnitude greater than other mineral references, supporting potential space charge effects preventing cholesterol ions from reaching the detector. Conversely, once the limit of detection has been reached and the S/N is zero, for all subsequent molarities lower than the limit of detection will produce a lower plateau. Because this dataset is small, and regressions excluded data points with S/N < 3, the details of a sigmoidal curve cannot be fit, making linear regressions the best alternative.

MINERAL	John Klein	Cumberland	Confidence H.	Mojave2	Marimba2	Quela	Sebina	Duluth	Stoer	Rock Hall	Aberlady	Kilmarie	Glen Etive 1	Glen Etive 2	Hutton	Glasgow
OPALINE																
AMORPHOUS	28 (15)	31 (18)	39 (15)	53 (15)	40 (20)	52 (26)	51 (25)	35 (15)	35 (15)	34 (15)	41 (20)	44 (20)	38 (19)	37 (19)	37.5 (19)	47 (23)
CLAY	22 (11)	18 (9)	7.6 (3.8)	4.7 (2.4)	23 (12)	16 (8)	19 (10)	15 (7)	10 (5)	13 (6)	28 (12)	28 (12)	34 (17)	26 (13)	6.3 (1.9)	24 (12)
PLAGIOCLASE			38.3 (4.3)	55.7 (3.8)	45.8 (3.6)	44 (2)	38.4 (2.4)	55.8 (1.8)	44.1 (1.7)	38.2 (4.1)	34.7 (3.8)	32.5 (3.6)	40 (2.8)	63 (3.1)	49.7 (6.4)	50.4 (3.5)
ANDESINE	43.8 (3.6)	43.6 (2.7)														
SANIDINE	1.7 (1.8)	3.1 (1.7)			7.7 (2.5)	6.1 (1.6)	5.1 (2)	9 (0.9)	4 (0.7)		3.9 (1.6)	2.3 (2)	5 (2.4)	6 (1.5)	4.7 (1.2)	3.7 (8.8)
ALBITE	2.7 (1.3)															
K-FELDSPAR			9.4 (1.3)													
PYROXENE					3.6 (3.7)	5.3 (1.6)	6.8 (4.2)	9 (1.4)	7.3 (1.3)	17.1 (1.9)	14.7 (5.6)	13.4 (4.6)	6 (1.9)	11 (2.6)	14.1 (2)	5.8 (3.7)
AUGITE	8.5 (3.4)	8.1 (2.5)	12 (4.1)	5.2 (5.2)												
PIGEONITE	12.7 (4)	15.6 (3.5)	9.9 (3.2)	10.9 (1.7)												
ENSTATITE																
ORTHOPYROXENE	6.8 (3.1)	8.1 (3.1)	3.9 (5.8)													
OLIVINE																
Fe-FORSTERITE																
FORSTERITE	5.1 (3.3)	1.8 (1.6)	2.3 (1.3)	0.5 (1.9)	5.3 (1.6)	5.1 (1.8)	3 (1)									
MAGNETITE	7 (1.9)	8.7 (1.9)	5.6 (1.3)	7.1 (1.4)				1.6 (0.3)	0.7 (0.2)		1.9 (1.1)				12.4 (3.4)	
HEMATITE	1.2 (0.9)	1.3 (1)	12.8 (2.8)	7.1 (1.4)	16.4 (2.1)	20 (1.5)	20.4 (1.7)	13 (0.8)	28.3 (1)	5.4 (0.4)	5.5 (1.4)	3.8 (1)	7 (2.5)	4 (1.3)	4.8 (1.2)	13.4 (3.1)
ILMENITE		1 (0.9)														
AKAGANEITE	2.4 (1.4)	3.4 (1.3)							1.6 (0.1)	11.3 (0.9)						
GOETHITE																
QUARTZ	0.6 (0.7)	0.2 (0.3)	1.3 (0.9)	1.9 (0.7)	1.2 (1)	1.1 (0.6)	1.2 (0.6)	1.3 (0.2)	1.5 (0.3)		2.1 (1)	0.8 (0.4)	2 (0.8)	2 (0.2)		3.3 (2.8)
CRISTOBALITE															9.3 (1.4)	0.7 (1)
TRIDYMITE																
ANHYDRITE	3.3 (2.1)	1.6 (1.2)			10.2 (1.1)	10.7 (0.8)	16.9 (1.1)	3 (0.5)	5.3 (0.5)	21.2 (2.6)	18.9 (2.2)	29.3 (1.3)	34 (1.3)	10 (0.6)	1.2 (0.8)	18.5 (2.6)
HALITE	0.2 (0.3)	0.2 (0.3)														
GYPSUM					6.4 (1.1)	1.8 (1.3)	3.8 (1.3)	1.8 (0.1)	4.2 (0.3)							
BASSANITE	2 (0.9)	1.4 (0.7)			1.9 (0.8)	4.5 (0.9)	1.8 (0.5)	5.4 (0.4)	0.8 (0.3)		18.4 (1.4)	10 (1)	3 (1.2)	3 (0.8)		3.2 (1.9)
PYRITE	0.4 (0.5)															
PYRRHOTITE	1.5 (1.5)	1.9 (1.1)														
JAROSITE			2.1 (1.3)	7.3 (3.8)	1.5 (0.5)	1.4 (0.6)	2.6 (0.6)		2.2 (0.3)	4.3 (0.9)						
APATITE			2.4 (2.8)	4.3 (2.4)						2.5 (0.8)					3.8 (1.8)	1 (1.8)
FLUORAPATITE																
Fe-carbonate																
SIDERITE												8 (1)	3 (0.9)			
ANKERITE																

Table S1: Data collected from the CheMin Open Database Repository used in this study for comparisons to Lake Sandvatn. Colors represent the groupings used for the comparison calculation. Uncertainties are those calculated by the CheMin team and listed in parentheses.

	10 cm (R = 3.43%)	28 cm (R = 3.94%)	40 cm (R = 3.73%)	47 cm (R = 3.86%)	57 cm (R = 3.32%)	66 (R = 3.77%)
Augite	**21.2** - 35.7 (0.3)	20.4 - **21.0** (0.3)	**19.5** - 29.9 (0.3)	**14.8** - 33.5 (0.3)	18.8 - **19.2** (0.2)	**18.8** - 34.5 (0.2)
Bytownite	**7.7** - 13 (0.5)	12.4 - **12.8** (0.5)		**0.9** - 2.0 (0.2)	4.4 - **4.6** (0.4)	**12** - 21.9 (0.6)
Labradorite	**12.3** - 20.8 (0.5)	17.4 - **17.8** (0.5)	**22.2** - 37.1 (0.3)	**21.2** - 47.9 (0.3)	18.2 - **18.5** (0.4)	**16.6** - 30.4 (0.6)
Forsterite	**8.7** - 14.7 (0.2)	6.2 - **6.4** (0.2)	**9** - 11.2 (0.2)	6.5 - **14.7** (0.2)	8.1 - **8.3** (0.2)	**6.7** - 12.2 (0.2)
Hematite	0.1 - 0.1 (0.0)	**0.4** - 0.5 (0.1)	**0.3** - 0.8 (0.1)	**0.8** - 1.7 (0.1)	0.5 - 0.5 (0.1)	**0.6** - 1.1 (0.1)
Nontronite	0.1 - 0.1 (0.1)		0 - **0.1** (0.1)	0.1 - 0.1 (0.1)		
Amorphous	15.5 - **49.8** (0.6)	**41.6** - 43.0 (0.7)	20.8 - **48.8** (0.4)	0 - **55.7** (0.4)	**48.9** - 49.9 (0.6)	0 - **45.3** (0.7)

88 cm (R = 4.04%)	118 (R = 3.63%)	130 cm (R = 3.64%)	147 cm (R = 3.96%)	157 cm (R = 2.83%)	168 cm (R = 3.39%)
20.5 - 37.4 (0.3)	**25.8** - 30.6 (0.3)	**21.5** - 36.6 (0.3)	**25.1** - 33.1 (0.3)	**13.3** - 13.7 (0.2)	**16.1** - 33.8 (0.2)
6.2 - 11.3 (0.6)	**13.0** - 15.4 (0.3)	**8.9** - 15.0 (0.4)	**12.0** - 15.9 (0.6)		**12.0** - 24.5 (0.5)
19.3 - 35.2 (0.6)	**15.0** - 23.7 (0.5)	**14.4** - 23.0 (0.4)	**19.8** - 28.4 (0.6)	**20.1** - 20.8 (0.2)	**15.2** - 31.4 (0.5)
8.0 - 14.6 (0.6)	**7.0** - 8.2 (0.2)	**5.3** - 7.8 (0.2)	**5.0** - 6.4 (0.2)	**2.9** - 3.0 (0.2)	**4.6** - 9.3 (0.2)
0.8 - 1.5 (0.1)	**0.5** - 0.6 (0.5)	0 - **0.1** (0.1)	0 - **0.2** (0.0)		**0.6** - 1.0 (0.1)
		0.1 - 0.3 (0.1)	0.2 - 0.2 (0.1)		
0 - **45** (0.8)	21.4 - **38.7** (0.6)	17.3 - **49.8** (0.6)	16.1 - **37.7** (0.8)	62.4 - **63.7** (0.3)	0 - **51.4** (0.7)

Table S2: XRD results for samples from SV22-24-core75. Bolded values indicate the original refinement results where the internal standard was set to 20 wt % and other values are the re-run refinements without defining the internal standard value. Notably, amorphous material is much more difficult to constrain and include in the refinements without the presence of an internal standard. Uncertainties are listed in parentheses as those produced from Jade during the first refinement.

	Bulk Geochemistry											
Core Depth	10 cm	28 cm	40 cm	47 cm	57 cm	66 cm	88 cm	118 cm	130 cm	147 cm	157 cm	168 cm
SiO2	47.93	48.47	47.80	48.19	48.11	48.08	48.13	48.28	48.93	48.60	47.44	47.40
TiO2	1.64	1.36	1.48	1.53	1.46	1.42	1.46	1.62	1.66	1.70	2.58	1.68
Al2O3	14.91	17.30	14.90	15.32	15.35	16.47	15.44	15.99	15.59	16.19	18.27	20.14
FeO*	12.34	10.55	12.02	11.98	11.79	11.25	11.68	11.33	11.79	11.43	13.23	11.70
MnO	0.21	0.18	0.20	0.20	0.20	0.19	0.20	0.20	0.21	0.21	0.21	0.19
MgO	9.37	7.79	9.75	9.13	9.04	8.43	8.92	8.16	7.96	7.68	5.38	5.67
CaO	11.39	12.14	11.72	11.41	11.81	12.01	11.96	12.27	11.42	11.85	10.03	10.93
Na2O	1.86	1.92	1.88	1.92	1.97	1.89	1.95	1.84	1.98	1.95	2.18	1.94
K2O	0.21	0.17	0.14	0.19	0.15	0.14	0.14	0.17	0.31	0.25	0.37	0.17
P2O5	0.14	0.11	0.11	0.13	0.12	0.11	0.12	0.13	0.16	0.16	0.32	0.17

Table S3: Bulk geochemistry results for SV22-24-core75. Constraints on uncertainties can be found in Johnson, Hooper, and Conrey (1999).

	Amorphous Geochemistry											
Core Depth	10 cm	28 cm	40 cm	47 cm	57 cm	66 cm	88 cm	118 cm	130 cm	147 cm	157 cm	168 cm
SiO2	39.38	41.05	39.11	42.90	40.02	39.95	39.16	38.49	42.96	39.19	43.03	41.90
TiO2	3.29	3.27	3.03	2.75	2.99	3.14	3.23	4.19	3.34	4.51	4.05	3.26
Al2O3	17.85	18.43	16.74	15.48	17.28	17.35	17.46	19.11	17.07	17.26	19.38	22.57
FeO*	19.38	18.73	18.90	16.77	18.20	18.57	18.80	20.62	18.85	22.77	18.58	18.11
MnO	0.42	0.43	0.41	0.36	0.41	0.42	0.44	0.52	0.42	0.56	0.33	0.37
MgO	9.87	9.24	11.21	10.67	10.17	10.46	10.35	9.03	8.34	9.16	4.86	5.24
CaO	7.24	6.17	8.26	8.80	8.56	8.23	8.40	5.48	6.10	3.95	6.81	6.06
Na2O	1.88	2.01	1.83	1.70	1.83	1.34	1.58	1.80	1.98	1.52	1.87	1.83
K2O	0.42	0.41	0.29	0.34	0.31	0.31	0.31	0.44	0.62	0.66	0.58	0.33
P2O5	0.28	0.26	0.22	0.23	0.25	0.24	0.27	0.34	0.32	0.42	0.50	0.33

Table S4: Calculated amorphous material composition for samples from SV22-24-core75.

Honor Code: I pledge on my honor that I have not given or received any unauthorized assistance on this assignment/examination.

Madeline Raith